Lawrence Berkeley National Laboratory
Lawrence Berkeley National Laboratory

Title
DIRECT EVIDENCE FOR CHARMED PARTICLES IN e+e- ANNIHILATION AT SPEAR

Permalink
https://escholarship.org/uc/item/4zz8348g

Author
Nguyen, H.K.

Publication Date
1977-04-01

eScholarship.org Powered by the California Digital Library
University of California

0 0 0 0 4 7 0 9 8 2 6

Invited Talk at the XIIth Rencontre
de Moriond, Flaine, Haute-Savoie,
France, March 6 - 18, 1977

LBL-6146
c.1

DIRECT EVIDENCE FOR CHARMED PARTICLES IN e^+e^- ANNIHILATION AT SPEAR

RECEIVED
LAWRENCE
BERKELEY LABORATORY

MAY 24 1977

LIBRARY AND
DOCUMENTS SECTION

Huu Khanh Nguyen

April 1977

Prepared for the U. S. Energy Research and
Development Administration under Contract W-7405-ENG-48

For Reference

Not to be taken from this room

LAWRENCE BERKELEY LABORATORY
UNIVERSITY OF CALIFORNIA
BERKELEY

LBL-6146
c.1

LEGAL NOTICE

This report was prepared as an account of work sponsored by the United States Government. Neither the United States nor the United States Energy Research and Development Administration, nor any of their employees, nor any of their contractors, subcontractors, or their employees, makes any warranty, express or implied, or assumes any legal liability or responsibility for the accuracy, completeness or usefulness of any information, apparatus, product or process disclosed, or represents that its use would not infringe privately owned rights.

0 0 0 0 4 7 0 7 8 2 7

LBL-6146

DIRECT EVIDENCE FOR CHARMED PARTICLES IN e^+e^- ANNIHILATION AT SPEAR

Huu Khanh NGUYEN*
Lawrence Berkeley Laboratory
University of California
Berkeley, California 94720 (USA)

Abstract: We study the properties of the new mesonic neutral and charged states with mass $M \sim 1865$ MeV/c^2 recently discovered in e^+e^- annihilation at SPEAR. We show that these states possess the characteristics expected for low-lying charmed mesons.

Résumé: Nous étudions les propriétés des nouveaux mésons neutres et chargés de masse $M \sim 1865$ MeV/c^2 découverts récemment dans les annihilations e^+e^- à SPEAR. Nous montrons que ces états possèdent les caractéristiques attendues pour les mésons charmés.

*Permanent address: LPNHE, University of Paris VI, Paris, France.

INTRODUCTION

Much progress has been made since the discovery[1] of the narrow neutral state at 1865 MeV/c^2 decaying to $K^{\pm}\pi^{\mp}$ and $K^{\pm}\pi^{\mp}\pi^{+}\pi^{-}$ in e^+e^- annihilation at SPEAR in May 1976. All the results obtained converge to confirm that we have observed direct production of nonzero charm mesons. Before describing these results in detail, I will review briefly the main properties predicted for low-lying charmed mesons.

I. PREDICTED PROPERTIES OF CHARMED MESONS

A fourth quark, c, with a new quantum number, charm, has been added to the three conventional quarks u, d and s by Bjorken and Glashow[2] to restore quark-lepton symmetry and by Glashow, Iliopoulos and Maiani[3] to explain the absence of neutral currents in the K decay ($K^o \not\to \mu^+\mu^-$ or $K \not\to \pi\nu\bar{\nu}$). As a consequence, the SU(3) multiplets describing known hadronic states, became SU(4) multiplets with a larger number of states; hence new hadrons are predicted.[4,5] In particular, one expects a charmed pseudoscalar isodoublet of mesons (D^o, D^+) and an isodoublet of charmed vector mesons (D^{*o}, D^{*+}).

A. Mass Prediction for D and D^*

Recently based on the measured mass of the ψ/J, more precise mass predictions for D and D^* have been calculated. Using an asymptotically free Gauge theory De Rujula, Georgi and Glashow[4] (DGG) have obtained: $M_{D^o} = (1830 \pm 30)$ MeV/c^2. Taking into account electromagnetic mass splitting, they show that:

$$M_{D^+} - M_{D^o} \cong M_{D^{*+}} - M_{D^{*o}} \cong 15 \text{ MeV}/c^2 \quad .$$

The hyperfine splitting calculation gives: $M_{D^*} - M_D \cong 130$ MeV/c^2. On the other hand Lane and Weinberg[6] have obtained:

$$m_{D^+} - m_{D^o} \cong 6.7 \text{ MeV}/c^2 \quad .$$

B. Width of the Charmed Particles

Since charm is conserved in strong and electromagnetic interaction, just as strangeness, the least massive charmed particles must decay weakly and would have very narrow width typical of the weak decay.

C. Favored Decay Products of D and D^*

In the standard charm model, Cabibbo-allowed weak transitions ($\sim \cos\theta_c$) favor the transformation of a charmed quark to a strange quark; hence one expects to observe kaons in the decay products of the D and D^*.

D. Existence of Exotic Final States

Furthermore, the decays of charmed particles obey the $\Delta C = \Delta S$ rule. Hence, for example, the D^+ meson which has $C = +1$ and $S = 0$ is favored to decay to $K^-\pi^+\pi^+$ rather than $K^+\pi^+\pi^-$. The $K^-\pi^+\pi^+$ final state, possessing $S = -1$ and $Q = +1$, is exotic because it cannot be formed from an s quark and a $\bar{u}$ or $\bar{d}$ quark in the framework of SU(3).

E. Non-Conservation of Parity

For weak decay one expects parity violations which are in principle observable in the four-body decay of the D^0 meson by observation of nonvanishing pseudoscalar product of the three momenta.[7] An alternative way to demonstrate parity violation is to study the Dalitz plot of $D^\pm \to K^\mp\pi^\pm\pi^\pm$ events in light of the two-body decay mode $D^0 \to K^\pm\pi^\mp$, just as for the case of τ and Θ.

F. Associated Production

Another consequence of charm conservation in strong and electromagnetic interactions is charmed particles produced in these interactions must appear in pairs with opposite charm quantum numbers.

G. Predicted Spin-Parity for D and D^*

Due to the SU(4) breaking, it will be very difficult to settle theoretically that either the lowest lying charmed meson is pseudoscalar or vector. Some theorists[8] have suggested that the lightest charmed meson might be a vector meson. But the natural extension from SU(3) to SU(4), proposed by other theorists,[4,5] leads to the spin-parity assignment of 0^- and 1^- respectively for the ground and excited states D and D^* of charmed mesons.

II. DATA AND TECHNIQUES OF ANALYSIS

The data studied in this report are based on $\sim$ 80,000 hadronic events

produced in e^+e^- annihilation. About 1/3 of these events is taken at fixed $E_{cm} = 4.028$ GeV/c^2, ~ 1/3 at $E_{cm} = 4.414$ GeV/c^2 and the remaining in the energy region ranging between 3.7 and 4.7 GeV/c^2. These events are observed with the SLAC-LBL magnetic detector at SPEAR. The detector and the event selection procedures have been described.[9] I will recall only the particle identification technique using the time-of-flight information. The TOF system is composed of 48 Pilot Y scintillation counters viewed by Amperex 56 DVP photomultipliers. Its rms resolution is $\sigma_{TOF} \cong 0.4$ ns.

To observe charmed mesons, we have used two equivalent particle identification techniques: the weight method and the direct particle identification method. In the first method, each track is assigned two weights equal to the probabilities of being a pion or a kaon, as deduced from the measured momentum and a Gaussian TOF distribution. The mass combinations are then weighted by the product of probabilities corresponding to the mass assignment for each track. Details on this technique can be found in Ref. 10. In the second method, we have associated to each good track two following quantities:

$$\chi_\pi^2 = \left(\frac{t_\pi - t_{TOF}}{\sigma_{TOF}}\right)^2 \quad \text{and} \quad \chi_K^2 = \left(\frac{t_K - t_{TOF}}{\sigma_{TOF}}\right)^2 ,$$

where the time of flight $t_\pi(t_K)$ is calculated from the measured momentum assuming that the particle is a $\pi(K)$ and t_{TOF} is the time of flight measured by the TOF system.

The track is called a K if:

$$\chi_K^2 < \chi_\pi^2 \quad \text{and} \quad \chi_K^2 < 3 \quad ;$$

otherwise it is called a π.

These two methods give practically the same results (Fig. 1). The weight technique has been employed in Refs. 1 and 11; in this report we use only the direct identification technique which is simpler in practice.

III. OBSERVATION OF NARROW PEAKS

The first evidence for narrow bumps in the invariant mass of the $K^\pm\pi^\mp$ and

$K^{\pm}\pi^{\mp}\pi^{+}\pi^{-}$ systems was discovered in the sample of events in the energy region between 3.7 and 4.7 GeV/c^2. The existence of these bumps immediately appeared to be related to the ~ 4 GeV peak region in $R = \sigma_{hadron}/\sigma_{\mu^+\mu^-}$ (Fig. 2), which was expected by theorists to be the charm production threshold.[4,5] Hence we took two other samples of events at $E_{cm} = 4.028$ GeV/c^2 and at $E_{cm} = 4.414$ GeV/c^2.

Figure 3 shows the invariant mass spectra of $K^{\pm}\pi^{\mp}$, $K^{\pm}\pi^{\mp}\pi^{\mp}$ and $K^{\pm}\pi^{\mp}\pi^{+}\pi^{-}$ for the final sample. Before discussing these invariant mass distributions in detail, I would like to stress that the narrow states observed near 1870 MeV/c^2 are beautifully confirmed by our higher statistics total sample. Recall that we have also detected small bumps[1] in the mass spectra of the $\pi^+\pi^-$ and K^+K^- systems at ~ 1750 MeV/c^2 and ~ 1990 MeV/c^2 respectively. Since the typical time difference between the K and the π in the $K^{\pm}\pi^{\mp}$ signal is only ~ 0.70 ns and our TOF resolution is ~ 0.4 ns, we can demonstrate by Monte-Carlo simulations that these bumps are due to the K-π misidentification and consistent with the entire signal being $K^{\pm}\pi^{\mp}$. We do not see any structure in the $\pi^{\pm}\pi^{+}\pi^{-}$ or $K^+K^-\pi^{\mp}$ mass combinations corresponding to the reflection of the $K^{\pm}\pi^{\mp}\pi^{\mp}$ signal, nor in the $\pi^-\pi^+\pi^-\pi^+$ or the $K^+K^-\pi^+\pi^-$ combinations corresponding to the $K^{\pm}\pi^{\mp}\pi^{+}\pi^{-}$ signal. This is understandable by the fact that in these cases the final particles have lower momentum than that of the $K^{\pm}\pi^{\mp}$ signal and the K-π discrimination is more efficient.

In the total sample we have estimated for the observed signals:

$$N_{K^{\pm}\pi^{\mp}} = 546 \pm 50 \quad , \quad N_{K^{\pm}\pi^{\mp}\pi^{\mp}} = 197 \pm 35 \quad \text{and} \quad N_{K^{\pm}\pi^{\mp}\pi^{+}\pi^{-}} = 333 \pm 55 \ .$$

These event numbers are not corrected for detection efficiency. (See V. Lüth talk for branching ratios of different channels.)

A preliminary analysis shows that the $K^{\pm}\pi^{\mp}\pi^{+}\pi^{-}$ signal is dominated by $K^{\pm}\rho^{o}\pi^{\mp}$ final state (Fig. 4). An appropriate Monte-Carlo calculation taking into account reflections and detection efficiency shows that the data is consistent with all of the $K^{\pm}\pi^{\mp}\pi^{+}\pi^{-}$ signal coming from $K^{\pm}\rho^{o}\pi^{\mp}$ decay mode, but less than 10% proceeding via $K^{*o}\pi^{+}\pi^{-}$ and less than 15% via $K^{*o}\rho^{o}$.

In Fig. 5 we present the invariant mass spectrum of the $K_S^o\pi^+\pi^-$ decay mode. A good signal near 1865 MeV/c^2 is observed. Details in $K_S^o \to \pi^+\pi^-$ selection is given in the V. Lüth talk.

To determine the characteristics of the new states, we prefer to use only the data taken at 4.028 GeV/c^2 which is, as we will see in Sections V and VI, near the threshold of $D\bar{D}^*$ and $D^*\bar{D}^*$ production. At this threshold energy the ratio background/signal is minimal. We have fitted the invariant mass distributions at 4.028(Fig. 6) with a Gaussian for the peak and a linear function for the background. The results are given in Table I where σ = HWHM/1.18.

Table I

Final state	Event number	Mass (MeV/c^2)	σ (MeV/c^2)
$K^\pm\pi^\mp$	171 ± 15	1865 ± 2	20 ± 2
$K^\pm\pi^\mp\pi^\mp$	84 ± 17	1872 ± 3	12 ± 3
$K^o\pi^+\pi^-$	61 ± 14	1864 ± 8	26 ± 6
$K^\pm\pi^\mp\pi^+\pi^-$	93 ± 30	1868 ± 5	13 ± 5

The errors in this Table are statistical only. The systematic error on the mass is about 10 MeV/c^2. Note that the mass values given by these fits are in good agreement with those obtained through our analysis of the recoil spectra, described in Section VI. The widths observed for the signals are compatible with those expected from experimental resolution alone. We find at the 90% confidence level that the decay full width of the observed states is less than 40 MeV/c^2. As we have suggested,[1,11] due to the proximity of their mass, the signals in $K^\pm\pi^\mp$, $K_S^o\pi^+\pi^-$ and $K^\pm\pi^\mp\pi^+\pi^-$ systems can be interpreted as the neutral decays of the same particle, and the signal in the $K^\pm\pi^\mp\pi^\mp$ system having similar mass is its charged partner.

So far, we have established that the observed states have a K in their decay products, a narrow width and a mass value in the region of ~ 1870 MeV/c^2. These properties are expected for the lowest lying charmed meson (Sec. IA,B,C).

I will discuss the exotic nature of the peak in the $K^{\pm}\pi^{\mp}\pi^{\mp}$ system in the next section.

IV. EVIDENCE FOR EXOTIC FINAL STATE

Due to experimental resolution and limited statistics of the first sample of our data ($3.7 < E_{cm} < 4.7$ GeV/c^2), the existence of the exotic charged state $K^{\pm}\pi^{\mp}\pi^{\mp}$ (see Section I-D) could not be established. However a highly significant signal is seen with the data taken at $E_{cm} = 4.028$ GeV/c^2 (Fig. 6), and at $E_{cm} = 4.414$ GeV/c^2. On the other hand, we do not see any significant structure in the nonexotic $K^{\pm}\pi^{\mp}\pi^{\pm}$ mass spectrum, nor in the triply-charged $K^{\pm}\pi^{\pm}\pi^{\pm}$. Also no corresponding bump is seen in doubly-charged systems such as $K^{\pm}\pi^{\pm}$, $K^{\mp}\pi^{\mp}\pi^{+}\pi^{-}$ or $K^{\pm}\pi^{\mp}\pi^{\pm}\pi^{\pm}$.

Recall that if the $K^{\pm}\pi^{\mp}\pi^{\mp}$ peak were due to the strong decay of a strange resonant state K^*, the isospin of this resonance would be 3/2 or 5/2 and the doubly charged decay modes are expected. But these modes have not been seen and one has never observed K^* with isospin larger than 1/2.

The observation of the exotic mode, $K^{\pm}\pi^{\mp}\pi^{\mp}$, and the absence of the nonexotic mode, $K^{\pm}\pi^{\mp}\pi^{\pm}$, constitutes an important step in identifying this state with the $D^{\pm}$.

V. CONSERVATION OF CHARM QUANTUM NUMBER

In this Section I will illustrate the conservation of the charm quantum number in e^+e^- annihilation by showing that:

- the new states are produced exclusively in association with another state with the same or higher mass.
- there is threshold energy for their production.

A. Associated Production

As soon as the narrow peaks were detected in the invariant mass of the $K^{\pm}\pi^{\mp}$ and $K^{\pm}\pi^{\mp}\pi^{+}\pi^{-}$ systems, it was shown that these peaks are associated with similar structures at high mass in the missing mass recoiling against these systems. The missing mass MM is defined as:

$$MM^2 = E_{cm}^2 + M^2 - 2E_{cm}\sqrt{p^2 + M^2} \qquad (1)$$

where M is the invariant mass and p the momentum of the corresponding combination of final particles.

Figure 7 shows the strong correlation between the invariant mass and the recoil mass in the case of the $K^{\pm}\pi^{\mp}$ system for events with E_{cm} between 3.9 and 4.25 GeV/c^2: Two clusters are clearly seen.

The recoil mass spectra corresponding to the $K^{\pm}\pi^{\mp}$, $K^{\pm}\pi^{\mp}\pi^{\mp}$ and $K^{\pm}\pi^{\mp}\pi^{+}\pi^{-}$ signals for $E_{cm} = 4.028$ GeV/c^2 data are presented in Fig. 8, where the invariant mass cuts are defined. To minimize the smearing of the experimental resolution in Eq. (1), we have calculated the recoil mass by fixing $M = 1865$ MeV/c^2 for the neutral signal and $M = 1872$ MeV/c^2 for the charged signal, instead of using the experimental value of M. Furthermore, in the case of $K^{\pm}\pi^{\mp}\pi^{+}\pi^{-}$ (Fig. 8b) we have reduced considerably the background without altering the signal by selecting only the events with at least one combination of $\pi^{+}\pi^{-}$ inside the ρ^{o} region (this is consistent with the dominant decay mode $K^{\pm}\rho^{o}\pi^{\mp}$). The great similarity between the $K^{\pm}\pi^{\mp}$ and $K^{\pm}\rho^{o}\pi^{\mp}$ recoil mass spectra corroborates our hypothesis that the signals in $K^{\pm}\pi^{\mp}$ and $K^{\pm}\rho^{o}\pi^{\mp}$ systems are the neutral decays of the same particle.

For $E_{cm} = 4.028$ GeV/c^2 data, two narrow peaks are observed in the $K^{\pm}\pi^{\mp}$ and $K^{\pm}\rho^{o}\pi^{\mp}$ recoil mass spectra at ~ 2010 MeV/c^2 and at ~ 2150 MeV/c^2 and a small bump is seen near 1870 MeV/c^2 (Figs. 8a and 8b). In the $K^{\pm}\pi^{\mp}\pi^{\mp}$ recoil mass distribution (Fig. 8c) the peak near ~ 2010 MeV/c^2 shows up very nicely while the two other ones are less apparent, especially the highest peak.

These structures in recoil mass spectra have been interpreted by De Rujula, Georgi and Glashow,[4] and Lane and Eichten,[6] as the manifestation of the following quasi-two-body reactions (Fig. 9):

$$\begin{aligned} e^+e^- &\to D\bar{D} \\ &\to D\bar{D}^* \quad \text{or} \quad \bar{D}D^* \\ &\to D^*\bar{D}^* \end{aligned}$$

where D and D^* may be charged or neutral.

I will discuss in Section VI the results we have obtained by fitting the data at 4.028 GeV/c^2 assuming that this interpretation is valid.

Because of the narrowness of its width the peak at ~ 2150 MeV/c^2 could also be interpreted as another excited state. However this hypothesis can be excluded by the fact that for the 4.414 GeV/c^2 data, the corresponding peak becomes broader and shifted to higher mass, as one can see in Fig. 10 where the background estimated by adjacent invariant mass regions of the signal is subtracted.

In Fig. 10 we also have evidence for a new excited state(s) creating a sharp enhancement in the recoil mass spectrum near ~ 2430 MeV/c^2.

B. Production Threshold Effect

Another test of the associated production is to see if there is a threshold energy for the production of the new particles. For this we have utilized a sample of 350,000 hadronic events taken at ψ' energy (E_{cm} = 3.684 GeV/c^2) and 150,000 hadronic events taken at ψ energy (E_{cm} = 3.095 GeV/c^2). We estimate that about 15% of these events are produced via second-order electromagnetic interactions, as indicated by Diagrams 1 and 2, and the new states could be created in these events.

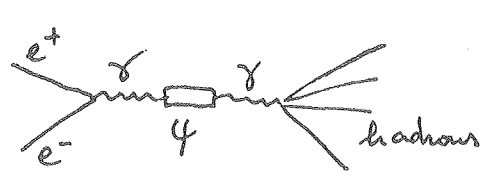

Diagram 1

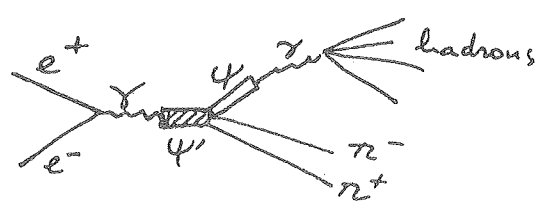

Diagram 2

In Fig. 11 are shown the $K^{\pm}\pi^{\mp}$ invariant mass spectra for E_{cm} = 3.095 GeV/c^2, E_{cm} = 3.684 GeV/c^2, E_{cm} = 4.028 GeV/c^2 and $3.9 < E_{cm} < 4.6$. We can note that the $K^{*o}(890)$ signal is seen in all spectra. But no evidence for $K^{\pm}\pi^{\mp}(1865)$ is observed for ψ and ψ' data, while for the events at E_{cm} = 4.028 GeV/c^2 the peak in the $K^{\pm}\pi^{\mp}$ system is very significant. This result suggests that the

production threshold energy for the new particle is larger than 3.1 GeV/c^2 and corroborates the hypothesis that it is produced in pair with the same or higher mass.

VI. MASS DETERMINATION AND BRANCHING RATIOS OF $D^* \to D\pi$ AND $D^* \to D\gamma$

From now on let us identify the narrow peaks in $K^{\pm}\pi^{\mp}$ and $K^{\pm}\rho^{o}\pi^{\mp}$ invariant mass distributions near 1865 MeV/c^2 with the charmed meson D^o, the charged peak at $\sim$ 1872 MeV/c^2 with the D^+ and the peak in recoil mass spectra near $\sim$ 2010 MeV/c^2 with the first excited charmed state D^*.

As we have suggested above, near threshold the charmed meson production can be well described by the three reactions:

$$e^+e^- \to D\bar{D} \qquad (a)$$

$$\to D\bar{D}^* \text{ or } \bar{D}D^* \qquad (b)$$

$$\to D^*\bar{D}^* \ . \qquad (c)$$

In a two-body reaction the masses of the two final particles are related directly to their momentum (Eq. 1). We have utilized this property to determine the mass of the D and the D^*. We have performed a global fit[12] of the total momentum spectra of $D^o \to K^{\pm}\pi^{\mp}$ and $D^{\mp} \to K^{\pm}\pi^{\mp}\pi^{\mp}$ for 4.028 GeV/c^2 data assuming that these arise from the primary D's of reactions (a) and (b) and secondary D's of reactions (b) and (c) with $D^* \to D\pi$ or $D^* \to D\gamma$. This global fit calculates the D and D^* mass in taking into account of the position of the reflection peaks as well as their width. It gives also the branching ratios $D^* \to D\pi$ and $D^* \to D\gamma$ and the proportions of reactions (a), (b) and (c).

In practice the fit proceeds as follows:

- the primary D's coming from reactions (a) and (b) are represented by delta functions.
- the decay of $D^* \to D\pi$ and $D^* \to D\gamma$ are assumed to be isotropic, so the secondary D's coming from D^* cascade decays have linear shapes of momentum distribution.[19]
- these momentum distributions are convoluted with the detector resolution and combined linearly with the background which is represented by a smooth

function estimated from the adjacent regions to the D signal.

The curve resulting from this global fit is shown in Figs. 12a and 12b.

We have also performed likelihood fits to the kinetic energy distributions of the D^o and $D^{\pm}$. This method gives very similar results. Table II summarizes the results deduced from the comparison of these two fits.

Table II

M_{D^o} =	1865 ± 3 MeV/c^2
M_{D^+} =	1872 ± 5 MeV/c^2
$M_{D^{*o}}$ =	2006 ± 2 MeV/c^2
$M_{D^{*+}}$ =	2010 ± 3 MeV/c^2
$\delta + \delta^*$ =	11 ± 5 MeV/c^2
$Q_{D^{*o} \to D^o \pi^o}$ =	6 ± 3 MeV/c^2

where: $\delta = M_{D^+} - M_{D^o}$ and $\delta^* = M_{D^{*+}} - M_{D^{*o}}$.

From the global fit the ratios of $e^+e^- \to D^o\bar{D}^o : D^o\bar{D}^{*o} + \bar{D}^o D^{*o} : D^{*o}\bar{D}^*$ are $1:9:11$ at $4.028\ \mathrm{GeV}/c^2$. Taking into account the spin-counting factors $1:4:7$ and p-wave phase space factors ($\sim p^3$), DGG[21] show that there is a surprisingly large production rate for $e^+e^- \to D^{*o}\bar{D}^{*o}$ at $E_{cm} = 4.028\ \mathrm{GeV}/c^2$.

For the cascade decays of the D^{*o} we have obtained:

$$\Gamma(D^{*o} \to D^o\gamma)/\Gamma(D^{*o} \to D^o\gamma \text{ and } D^* \to D^o\pi^o) \cong 0.5 \quad .$$

This value is in good agreement with that predicted by Ono[13] for example.

VII. NONCONSERVATION OF PARITY IN D DECAY

The details concerning this study has been published[14]; I will briefly summarize our results.

Since we observe the $D^o \to K^{\pm}\pi^{\mp}$ decay mode which is a natural spin-parity state ($J^P = 0^+, 1^-, 2^+$, etc.), an evidence for parity violation in the D decay is observed if the decay mode $D^{\pm} \to K^{\mp}\pi^{\pm}\pi^{\pm}$ is incompatible with a natural spin parity assignment.

Since three pseudoscalars cannot be in a $J^P = 0^+$ state, the observation

of the final state $D \to K\pi\pi$ excludes this spin parity assignment.

The cases of $J = 1^-$ and $J = 2^+$ can be ruled out by studying the population of the Dalitz plot of the $D^\pm \to K^\mp\pi^\pm\pi^\pm$. Figure 13 shows the Dalitz plots respectively for $D^\pm \to K^\mp\pi^\pm\pi^\pm$ and for the background represented by nonexotic combinations. Both of these are uniformly populated. The uniformity of the Dalitz plot density is inconsistent with a $K\pi\pi$ state of pure natural spin-parity, for which the Dalitz plot has to be depopulated at the boundary.

To evaluate this effect more quantitatively, the formalism of Zemach[20] has been used to calculate the simplest matrix elements. For $J = 1^-$ and $J = 2^+$, we have for unpolarized production:

$$I_{1^-} \propto |T_{\pi_1} - T_{\pi_2}|^2 |\vec{\pi}_1 \times \vec{\pi}_2|^2$$

$$I_{2^+} \propto |\vec{\pi}_1 - \vec{\pi}_2|^2 |\vec{\pi}_1 \times \vec{\pi}_2|^2$$

where I_{J^P} is the population density of the Dalitz plot, $\vec{\pi}$ is the pion momentum in the rest frame of the D and T_π is its kinetic energy. These densities have been utilized in Monte-Carlo simulations of $D \to K\pi\pi$ decay to predict Dalitz densities for these two hypotheses. Figure 14 shows the experimental $K\pi\pi$ invariant mass distributions for events within the shaded regions in the respective inserts. These regions have been defined so that for a phase space decay an equal number of events would be observed in the shaded area and in the non-shaded area. The boundary of these regions is contoured at a constant I_{J^P}. In both cases, $J^P = 1^-$ and $J^P = 2^+$, the experimental population is consistent with equal division, while the population divisions predicted for the peripheral to central region are 1 : 8.2 and 1 : 5.6 respectively. The $K\pi\pi$ data is therefore clearly incompatible with a pure natural spin-parity final state: 0^+, 1^- and 2^+. This result, together with the observed decay mode $D^0 \to K\pi$, suggest that the D's decay weakly as expected for charmed mesons.

VIII. SPIN-PARITY ANALYSIS[15]

Up to now we have shown that the new particles possess the properties expected for charmed mesons, but our discussion would not be complete without

discussion of their spin and parity. As mentioned in Sec. I-G, there is no obvious theoretical argument favoring a vector or pseudoscalar assignment for the lightest charmed meson; both of these spin assignments have their theorist-defenders. I will show in this section that the data favors the simplest hypothesis; i.e., $J = 0$ for the D and $J = 1$ for the D^* charmed mesons.

We have seen (Sec. VI) that near threshold the charmed meson production is dominated by the quasi-two-body reactions:

$$e^+e^- \rightarrow D\bar{D} \qquad (a)$$

$$\rightarrow D\bar{D}^* + \bar{D}D^* \qquad (b)$$

$$\rightarrow D^*\bar{D}^* \,. \qquad (c)$$

Jackson[17] and recently Gilman[18] have pointed out that the study of the angular distributions of the D^o decaying in $K^{\pm}\pi^{\mp}$ in these reactions may give information about the spin and parity of the D and D^*. Experimentally we can obtain nearly clean samples of events produced via reaction (b) and (c). The data used for this spin analysis consists of $\sim 35{,}000$ hadronic events taken near threshold ($3.9 < E_{cm} < 4.25$ GeV/c^2). All neutral 2-prong combinations are considered as potential $D^o \rightarrow K^{\pm}\pi^{\mp}$. The track having time-of-flight measurement most consistent with the K hypothesis is called K, the other track is called π.[16]

We study reaction (b) by cutting on invariant mass from 1820 to 1920 MeV/c^2 and on momentum from 515 to 615 MeV/c. We have obtained a sample of 153 D^o's of which 15% are estimated to be background two-prong combinations. As discussed in Sec. VI, the D^o's selected by this momentum cut come from three different sources within reaction (b): primary D^o's recoiling against $\bar{D}^{*o}$, secondary D^o's from $D^{*o} \rightarrow D^o\pi^o$ and secondary D^o's from $D^{*o} \rightarrow D^o\gamma$.

A sample of 110 events from reaction (c) are selected by cutting D^o momentum from 120 to 220 MeV/c. We estimate that the background is about 15% and the proportions of D^o coming from $D^* \rightarrow D^o\pi^o$ and $D^* \rightarrow D^o\gamma$ are $\sim 75\%$ and 25% respectively.

To compare the data with the predicted angular distributions, the effects of background and of secondary D^o's from D^{*o} decay, as well as the detection

efficiency, are included in the Monte-Carlo calculations.

In principle all values of spin are possible for the D and D^* but one would naturally expect the low-lying charmed states to have spins of less than two in light of the old spectroscopy (π-ρ, K-K^*, etc.). Hence we examine the three following spin-parity assignments:

J_D^P	$J_{D^*}^P$
$0^\pm$	$0^\pm$
$0^\pm$	$1^\pm$
$1^\pm$	$0^\pm$

using the data samples selected for reaction (b). Note that, in these spin assignments, the relative parity of the D and D^* is even. Of course, for spinless D and D^*, the production $e^+e^- \to D\bar{D}^*$ via a virtual photon implies that the relative parity of D and D^* is even. In addition the observation of the $D^* \to D\pi$ decay mode implies that the D and D^* must have even relative parity if one state has spin 1 and the other spin 0.

A. $J_D = 0^\pm$ and $J_{D^*} = 0^\pm$

For spinless D's and D^*'s of even parity, the expected polar distribution for primary D^0's in the reaction $e^+e^- \to D\bar{D}^* + \bar{D}D^*$ is given by:

$$\frac{d\sigma}{d\cos\Theta} \propto \sin^2\Theta \quad . \tag{4}$$

The dashed and dotted curve of Fig. 15 shows this predicted angular distribution. The experimental distribution is clearly incompatible with that expected for $J = 0^\pm$ and $J_{D^*} = 0^\pm$ with a χ^2 of 74 for 9 degrees of freedom and shows that the spinless assignment for both D and D^* is excluded. This spin assignment of the D and D^* is also ruled out by the observation of the mode $D^* \to D\gamma$ and $D^* \to D\pi$.

B. $J_D = 0^\pm$ and $J_{D^*} = 1^\pm$

In this case the direct D^0's have the production polar distribution[17]:

$$\frac{d\sigma}{d\cos\Theta} \propto 1 + \cos^2\Theta \quad . \tag{5}$$

This distribution represented by the solid curve in Fig. 15 is in good agreement with the experimental distribution (CL > 75%).

Furthermore the $D \to K\pi$ decay should be isotropic in the D helicity frame. The experimental polar helicity distribution for the decay kaon is shown in Fig. 16, where the solid curve is deduced from Monte-Carlo simulations. Again the data is consistent with the calculated distribution (CL > 50%).

C. $J_D = 1^{\pm}$ and $J_{D^*} = 0^{\pm}$

The dashed curve in Fig. 15 represents the expected production polar distribution for this spin assignment. The consistency with the data (CL ≅ 28%) is not as good as in the previous case, but could not exclude the $J_D^P = 1^{\pm}$ and $J_{D^*}^P = 0^{\pm}$ spin assignment. Note that, if efficiency were uniform over the angular variables, the solid and dashed curve in Fig. 15 would be identical. However we can exclude this spin hypothesis by the decay kaon helicity polar distribution (Fig. 16). The joint production and decay distribution for primary D^0's is given by[17]:

$$\frac{d\sigma}{d\cos\Theta\, d\cos\theta\, d\varphi} \propto \sin^2\theta(\cos^2\varphi + \cos^2\Theta\sin^2\varphi) \qquad (6)$$

where θ and φ are polar and azimuthal angles of the kaon in the D's helicity system. This distribution has been used in Monte-Carlo simulations to compute the expected helicity polar distribution. The predicted curve (dashed curve in Fig. 16) is inconsistent with the data with a χ^2 of 23 for 9 degrees of freedom (CL ≅ 0.6%).

We have devised an alternative method for comparing the data to the distribution of Eq. (5) and Eq. (6) which makes use of all three angular variables and handles backgrounds differently. The technique displays the invariant mass plot for events satisfying the momentum cut and having variables within one of two angular regions chosen to insure discrimination between Eq. (5) and (6) by dividing the space of angular variables by a surface of constant $I_3 = \sin^2\theta(\cos^2\varphi + \cos^2\theta\sin^2\varphi)$. Figures 18a and 18b show the $K^{\mp}\pi^{\pm}$ invariant mass distribution for events satisfying $I_3 < 0.32$ and $I_3 > 0.32$ respectively. The fit of Figs. 18a and 18b, consisting of a Gaussian signal over an exponen-

tially falling background, gives 58 ± 8 and 73 ± 10 signal events respectively. Defining an asymmetry variable α equal to the difference in the number of signal events over their sum, we obtain $\alpha = 0.11 \pm 0.10$ which is in good agreement with the value of 0.11 ± 0.02 expected for spin 0 D^0's and spin 1 D^*'s and inconsistent with 0.43 ± 0.02, the value obtained for spin 1 D^0's and spin 0 D^*'s ($\chi^2 = 10.2$, CL $= 2.10^{-3}$).

Furthermore we can utilize the sample selected for reaction (c) to study the $J_{D^*} = 0$ spin assignment. In this sample the majority of D^0's are from $D^* \rightarrow D\pi^0$, where small Q value ($Q \cong 6$ MeV/c^2) insures the observed D^0 polar angle lies close to the D^* polar angle. Hence we can use the D^0's polar production distribution instead of that which would be observed for D^*.

The predicted angular distribution for a pair of particles produced in e^+e^- annihilation is of the form:

$$\frac{d\sigma}{d \cos \Theta} \propto 1 + \alpha \cos^2 \Theta \qquad (7)$$

where α is a constant and equal to -1 in the case of spinless particles. The curve of Fig. 17 represents the fit of the experimental distribution with a linear combination of Eq. (7) for $D^* \rightarrow D\pi^0$ decays, the convoluted form of Eq. (7) for $D^* \rightarrow D\gamma$ decays and an isotropic background. We find $\alpha = -30 \pm 0.33$; this is 2.1 standard deviations from the value of $\alpha = -1$ expected for $J_{D^*} = 0$.

In summary the decay and production angular distributions for D^0's near threshold in reactions (b) and (c), together with the observation of the $D^* \rightarrow D\pi^0$ and $D^* \rightarrow D\gamma$ decay modes, show that our data is consistent with spin-parity assignment $0^\pm$, $1^\pm$ for the D and D^*, and inconsistent with $0^\pm$, $0^\pm$ and $1^\mp$, $0^\mp$. The first assignment with negative parity is the most natural assignment for the low-lying charmed mesons.

CONCLUSION

We have observed four new mesonic states, two neutral states at 1865 ± 3 MeV/c^2 and 2006 ± 2 MeV/c^2, and two corresponding charged states at 1872 ± 5 MeV/c^2 and at 2010 ± 3 MeV/c^2.

0 0 0 4 7 0 9 8 3 5

The presence of a kaon in their decay products, the observation of the exotic mode $K^{\pm}\pi^{\mp}\pi^{\mp}$, their weak decay (narrow width, violation of parity), their associated production, their production threshold behavior and their spin and parity suggest that they are indeed the long-sought low-lying charmed mesons D and D^*.

The results presented here are the work of the LBL-SLAC collaboration at SPEAR, whose other members are: G. S. Abrams, M. S. Alam, A. M. Boyarski, M. Breidenbach, W. C. Carithers, W. Chinowsky, S. Cooper, R. G. DeVoe, J. M. Dorfan, G. J. Feldman, C. E. Friedberg, D. Fryberger, G. Goldhaber, G. Hanson, J. Jaros, A. D. Johnson, J. A. Kadyk, R. R. Larsen, D. Lüke, V. Lüth, H. L. Lynch, R. J. Madaras, C. C. Morehouse, J. M. Paterson, M. L. Perl, I. Peruzzi, M. Piccolo, F. M. Pierre, T. P. Pun, P. Rapidis, B. Richter, B. Sadoulet, R. H. Schindler, R. F. Schwitters, J. Siegrist, W. Tanenbaum, G. H. Trilling, F. Vannucci, J. S. Whitaker, and J. E. Wiss.

I wish to thank G. Goldhaber and G. H. Trilling for their warm hospitality and Ms. C. Frank for her meticulous work in typing and compiling this report.

This work was supported by the U. S. Energy Research and Development Administration.

FOOTNOTES AND REFERENCES

1. G. Goldhaber, F. M. Pierre et al., Phys. Rev. Lett. 37, 255 (1976).
2. J. D. Bjorken and S. L. Glashow, Phys. Letters 11, 255 (1964).
3. S. L. Glashow, J. Iliopoulos and L. Maiani, Phys. Rev. D2, 1285 (1970).
4. A. De Rujula, H. Georgi and S. L. Glashow, Phys. Rev. D12, 147 (1975) and Phys. Rev. Lett. 37, 398 (1976).
5. M. K. Gaillard, B. W. Lee and J. L. Rosner, Rev. Mod. Phys. 47, 277 (1975); M. B. Einhorn and C. Quigg, Phys. Rev. D12, 2015 (1975).
6. K. Lane and S. Weinberg, Phys. Rev. Lett. 37, 717 (1976). See also H. Fritzsch, Phys. Rev. Lett. 63B, 419 (1976) and D. B. Lichtenberg, Phys. Rev. D12, 3760 (1975).

7. A. De Rujula, S. L. Glashow and R. Shankar, Phys. Rev. D14, 752 (1976).

8. G. Altarelli, N. Cabibbo and L. Maiani, Phys. Rev. Lett. 35, 635 (1975); S. Borchardt and V. S. Mathur, Phys. Rev. Lett. 36, 1287 (1976).

9. J.-E. Augustin et al., Phys. Rev. Lett. 34, 233 (1975); J.-E. Augustin et al., Phys. Rev. Lett. 34, 764 (1975).

10. G. Goldhaber, Study of Charmed Mesons at SPEAR, lectures at the Summer Institute on Particle Physics, Stanford, CA, August 1976, LBL-5534.

11. I. Peruzzi et al., Phys. Rev. Lett. 37, 569 (1976).

12. G. Goldhaber et al., to be published.

13. S. Ono, Phys. Rev. Lett. 37, 655 (1976).

14. J. E. Wiss, G. Goldhaber et al., Phys. Rev. Lett. 37, 1531 (1976).

15. H. K. Nguyen, J. E. Wiss et al., to be published.

16. For approximately 40% of these events this amounts to little more than a random selection. For the production angular distribution this K-π ambiguity is irrelevant; however it could matter in analyzing the decay distribution of the kaon in the D^0 helicity frame. Fortunately we find that it does not, since, for slow D^0's, K-π interchange effectively reverses the direction of the kaon in the D^0 helicity frame, and the angular distributions we are testing are invariant under this transformation.

17. J. D. Jackson, LBL note JDJ/76-1.

18. F. J. Gilman, private communication.

19. In fact decays of $D^* \to D\pi$, $D^* \to D\gamma$ can be shown to be anisotropic for the reaction (2), but this anisotropy has a negligible effect on the D^0 momentum spectrum.

20. C. Zemach, Phys. Rev. B133, 1201 (1964).

21. A. De Rujula, H. Georgi and S. L. Glashow, Molecular Charmonium: New Spectroscopy, HUTP-76/A176.

FIGURE CAPTIONS

Fig. 1. Invariant mass spectra of $K^{\pm}\pi^{\mp}$ and $K^{\pm}\pi^{\mp}\pi^{\mp}$. The dots are from direct identification and the histograms from weight method (see text).

Fig. 2. The ratio $R = \sigma_{hadron}/\sigma_{\mu^+\mu^-}$. The location of the two high-statistics points at 4.028 and 4.414 GeV/c^2 is also indicated.

Fig. 3. Invariant mass spectra of $K^{\pm}\pi^{\mp}$, $K^{\pm}\pi^{\mp}\pi^{+}\pi^{-}$ and $K^{\pm}\pi^{\mp}\pi^{+}\pi^{-}$ for final sample.

Fig. 4. (a) Invariant mass distribution of $K^{\pm}\rho^{o}\pi^{\mp}$, the ρ^{o} region is defined as $650 < M_{\pi^+\pi^-} < 850$ MeV/c^2. (b) $K^{\pm}\pi^{\mp}\pi^{+}\pi^{-}$ invariant mass distribution for events with both $\pi^{+}\pi^{-}$ combinations outside the ρ^{o} region.

Fig. 5. $K^{o}_{S}\pi^{+}\pi^{-}$ invariant mass spectrum for 4.03 GeV/c^2 data.

Fig. 6. Invariant mass spectra of $K^{\pm}\pi^{\mp}$, $K^{\mp}\pi^{\pm}\pi^{\pm}$ and $K^{\pm}\pi^{\mp}\pi^{+}\pi^{-}$ for 4.03 GeV/c^2 data.

Fig. 7. $K^{\pm}\pi^{\mp}$ invariant mass versus $K^{\pm}\pi^{\mp}$ missing mass for data with E_{cm} between 3.9 and 4.25 GeV/c^2.

Fig. 8. Recoil mass spectra against $K^{\pm}\pi^{\mp}$, $K^{\pm}\rho^{o}\pi^{\mp}$ and $K^{\pm}\pi^{\mp}\pi^{\mp}$ signals for 4.03 GeV/c^2 data.

Fig. 9. (a) Predicted recoil spectrum against D^{o}; (b) predicted recoil spectrum for $D^{\pm}$.

Fig. 10. (a) Recoil mass spectrum against $K^{\pm}\pi^{\mp}$ and $K^{\pm}\pi^{\mp}\pi^{+}\pi^{-}$ signals for 4.03 GeV/c^2 data, background subtracted. (b) Recoil mass spectrum against $K^{\pm}\pi^{\mp}$ and $K^{\pm}\pi^{\mp}\pi^{+}\pi^{-}$ signals for 4.4 GeV/c^2 data, background subtracted.

Fig. 11. $K^{\pm}\pi^{\mp}$ invariant mass distributions for ψ/J data, for ψ' data, for total sample and for 4.03 GeV/c^2 data.

Fig. 12. (a) Momentum distribution of $K^{\pm}\pi^{\mp}$ signal for 4.03 GeV/c^2 data. Solid curve is deduced from global fit. (b) Same distribution for the $K^{\pm}\pi^{\mp}\pi^{\mp}$ signal.

Fig. 13. (a) Dalitz plot for $K^{\pm}\pi^{\mp}\pi^{\mp}$ exotic signal; (b) Dalitz plot nonexotic final state $K^{\pm}\pi^{\mp}\pi^{\pm}$.

Fig. 14. Invariant mass distributions of $K^{\pm}\pi^{\mp}\pi^{\mp}$ inside shaded regions in respective inserts (see text).

Fig. 15. Production polar distribution of D^{o} in reaction (b). Dashed and dotted curve corresponds to spinless D and D^{*}. Solid curve corresponds to $J_D = 0^{\pm}$ and $J_D = 1^{\pm}$. Dashed curve corresponds to $J_D = 1^{\pm}$ and $J_{D^*} = 0^{\pm}$.

Fig. 16. Helicity polar distribution for D^{o} in reaction (b). Solid curve

corresponds to $J_D = 0^{\pm}$ and $J_{D^*} = 1^{\pm}$. Dashed curve corresponds to $J_D = 1^{\pm}$ and $J_{D^*} = 0^{\pm}$.

Fig. 17. Production polar distribution for D^0 in reaction (c). Solid curve is deduced from fit (see text).

Fig. 18. Invariant mass spectra of $K^{\pm}\pi^{\mp}$ system for $I_3 < 0.32$ and $I_3 > 0.32$.

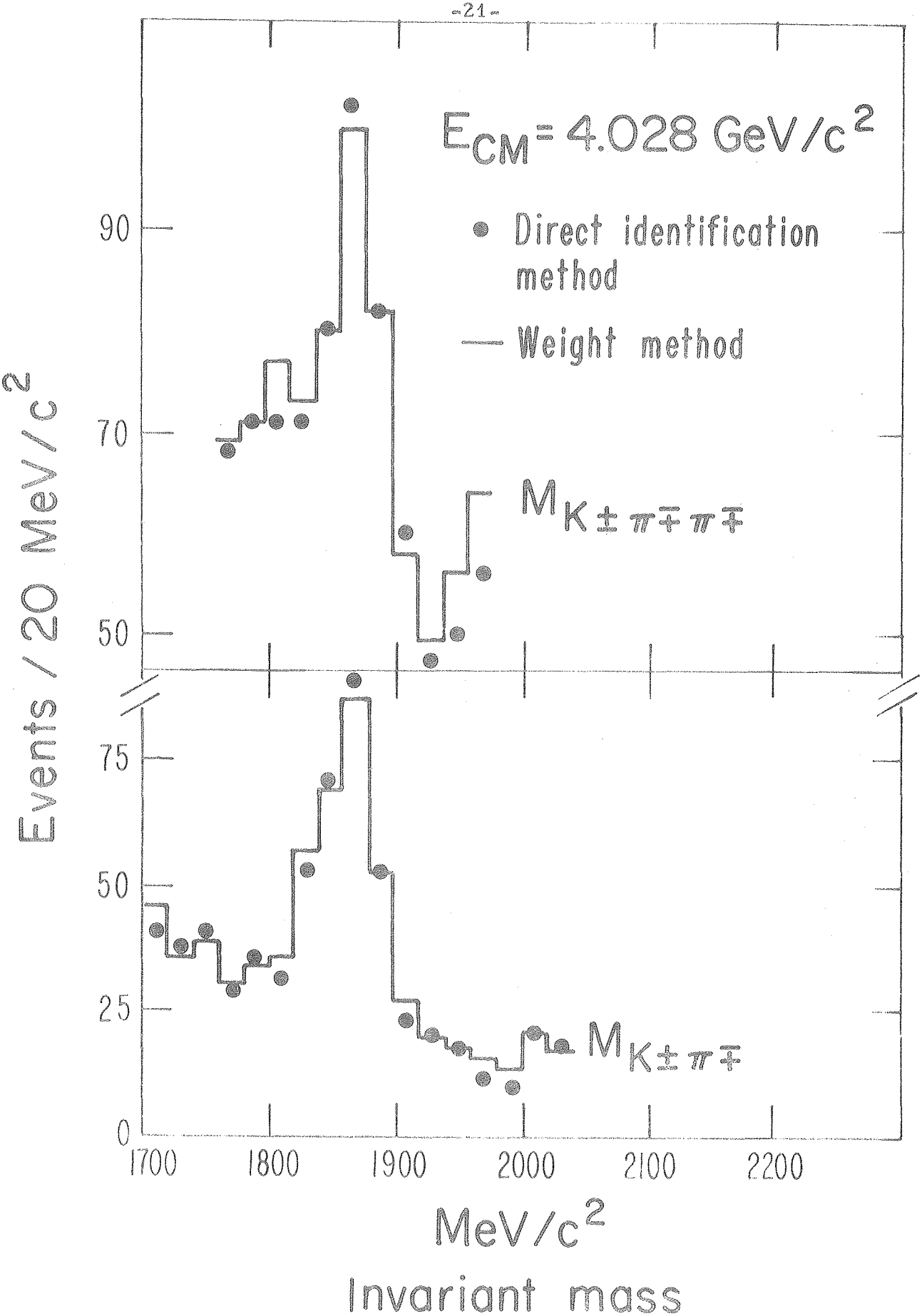

Fig. 1

XBL 772-416

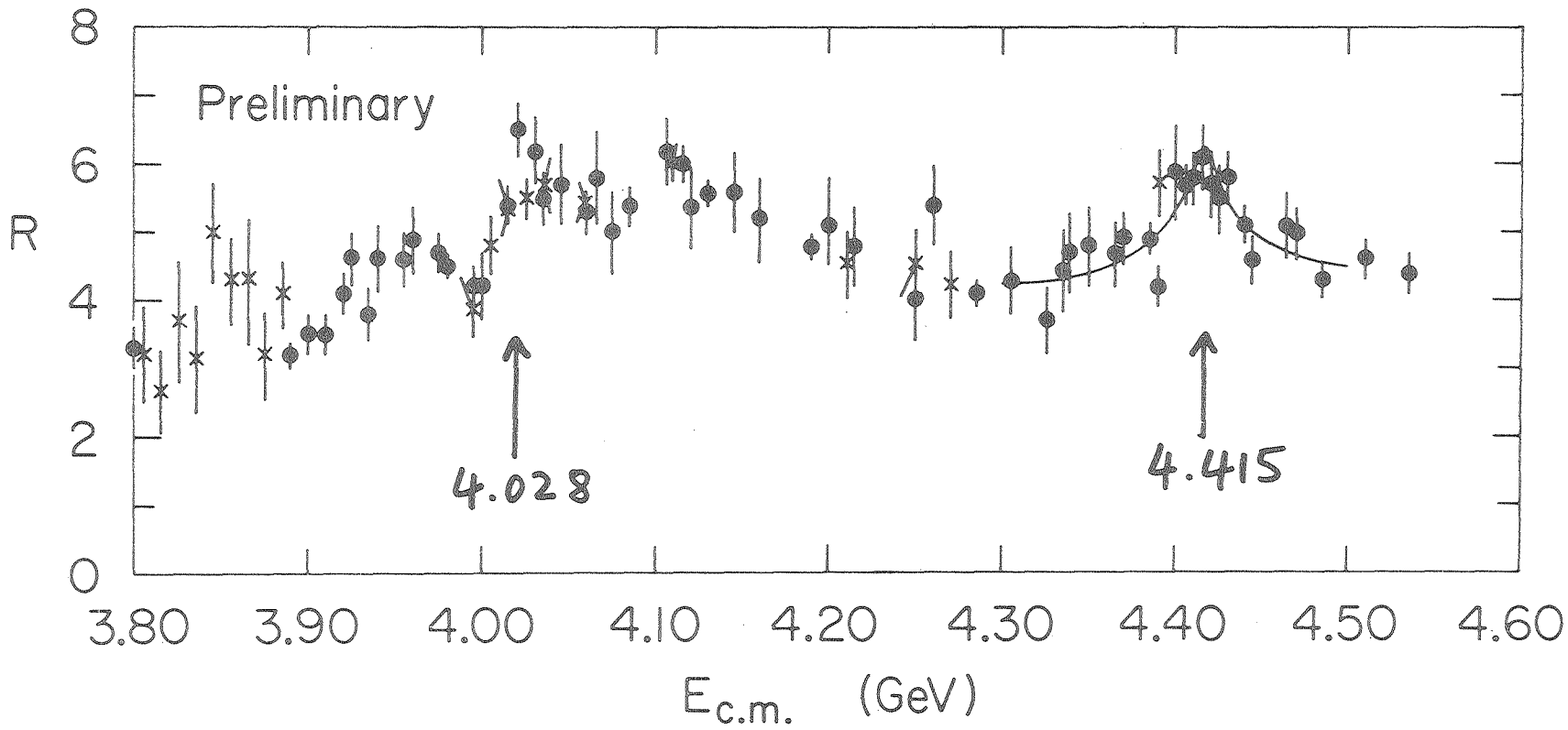

Fig. 2

XBL 767-8808

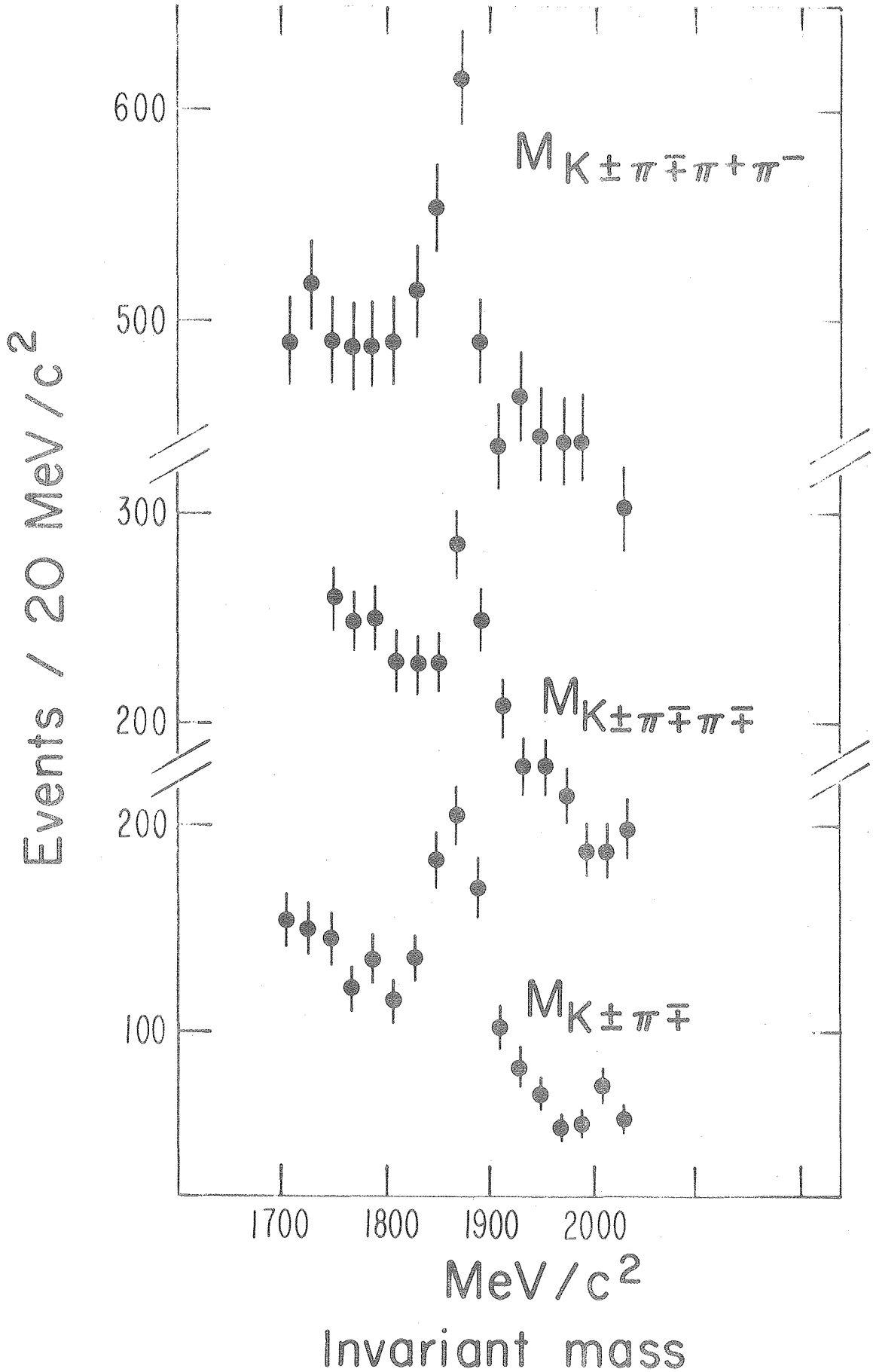

Fig. 3 XBL 772-415

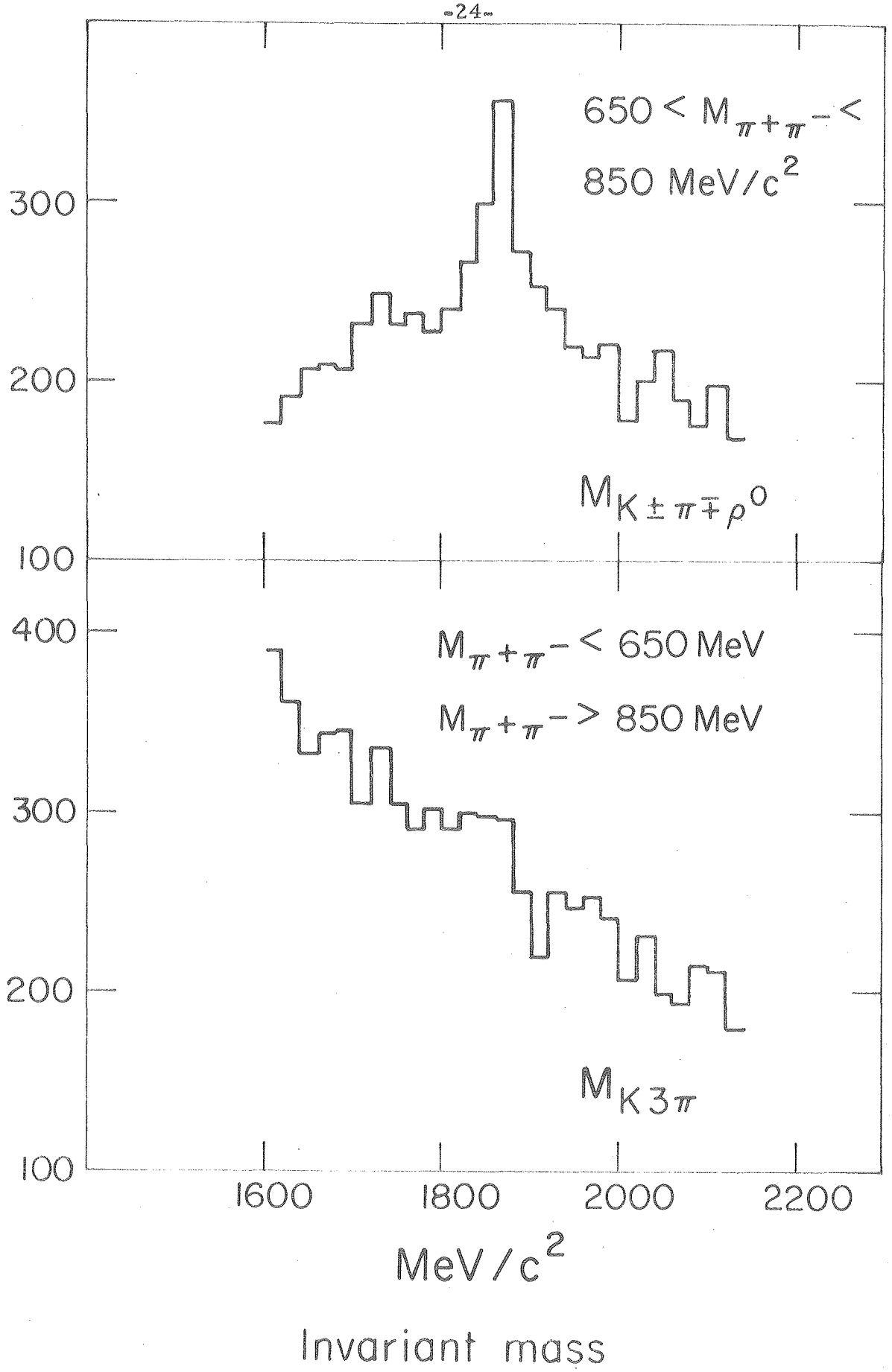

Fig. 4

XBL 772-413

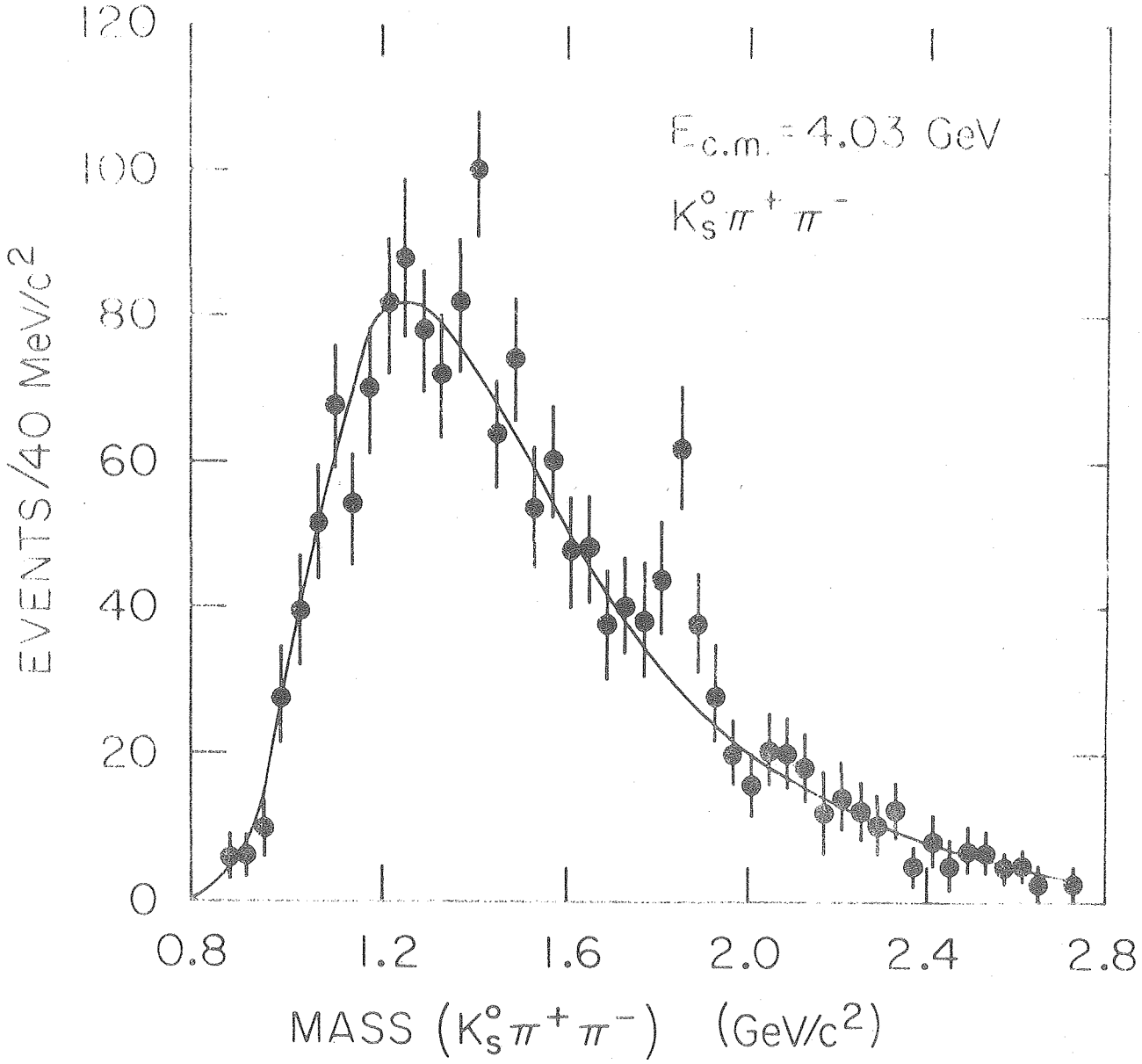

XBL 773-8208

Fig. 5

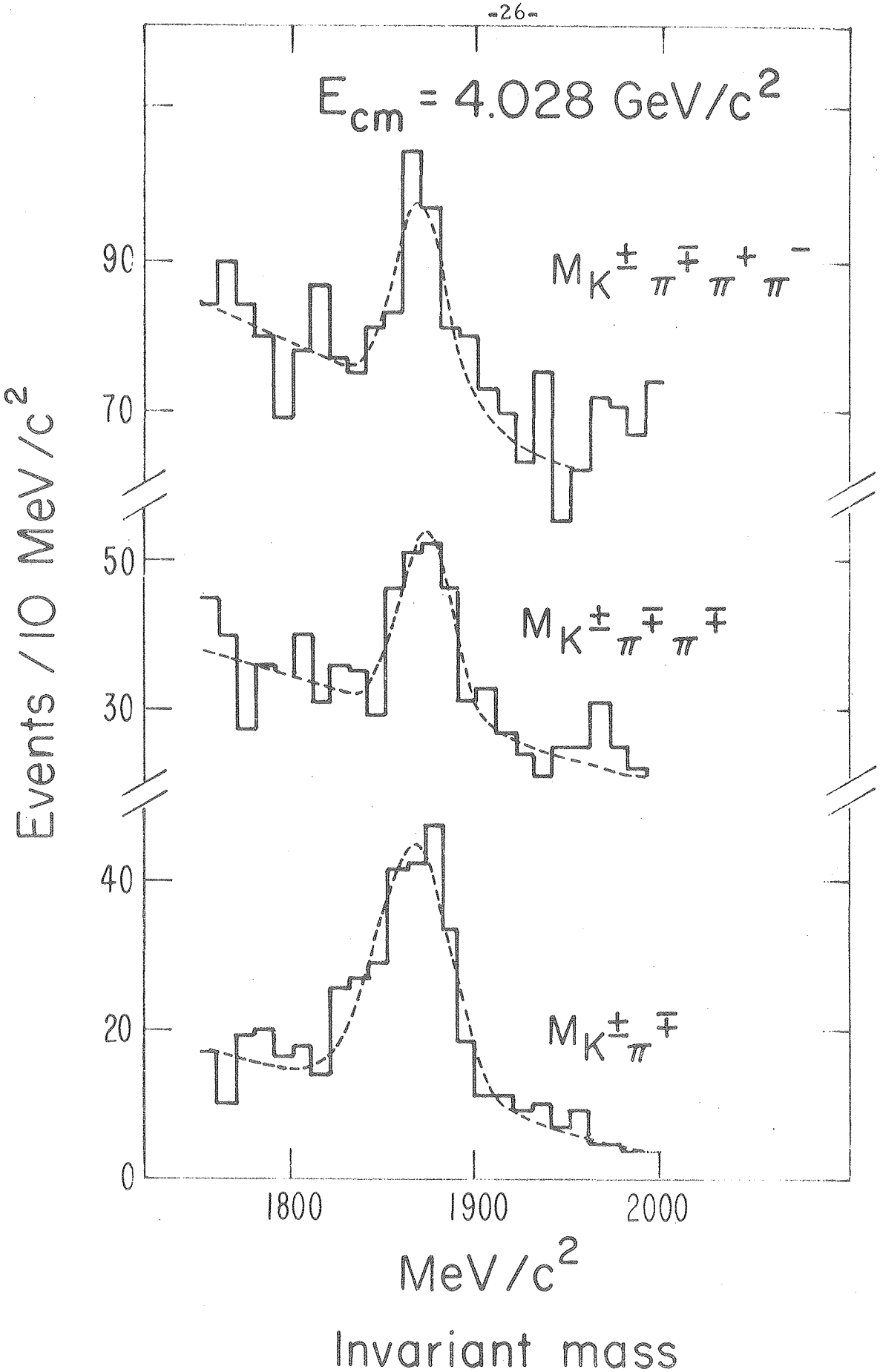

Fig. 6

XBL 772-411

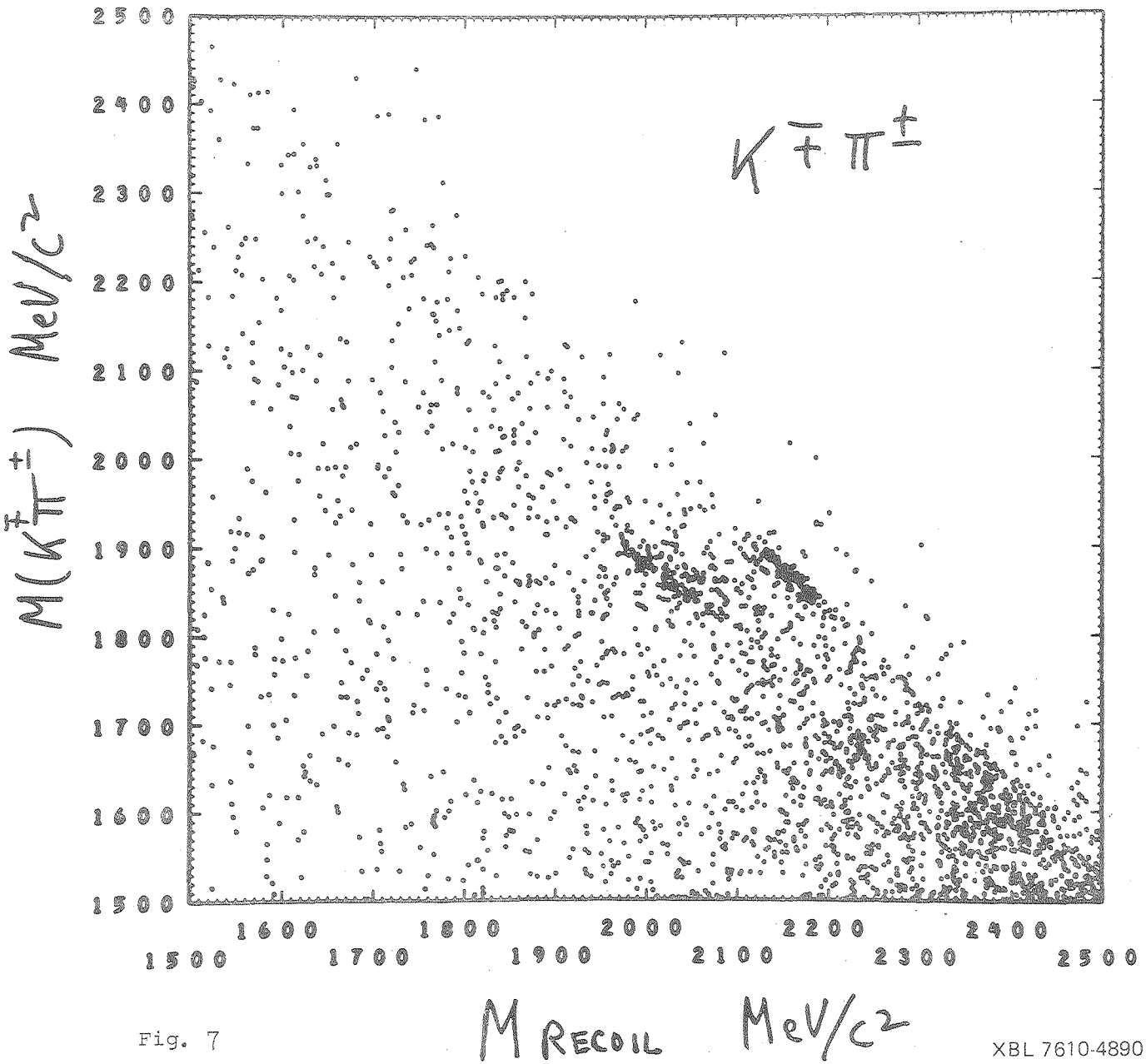

Fig. 7

XBL 7610-4890

0 0 1 0 4 7 0 9 8 4 0

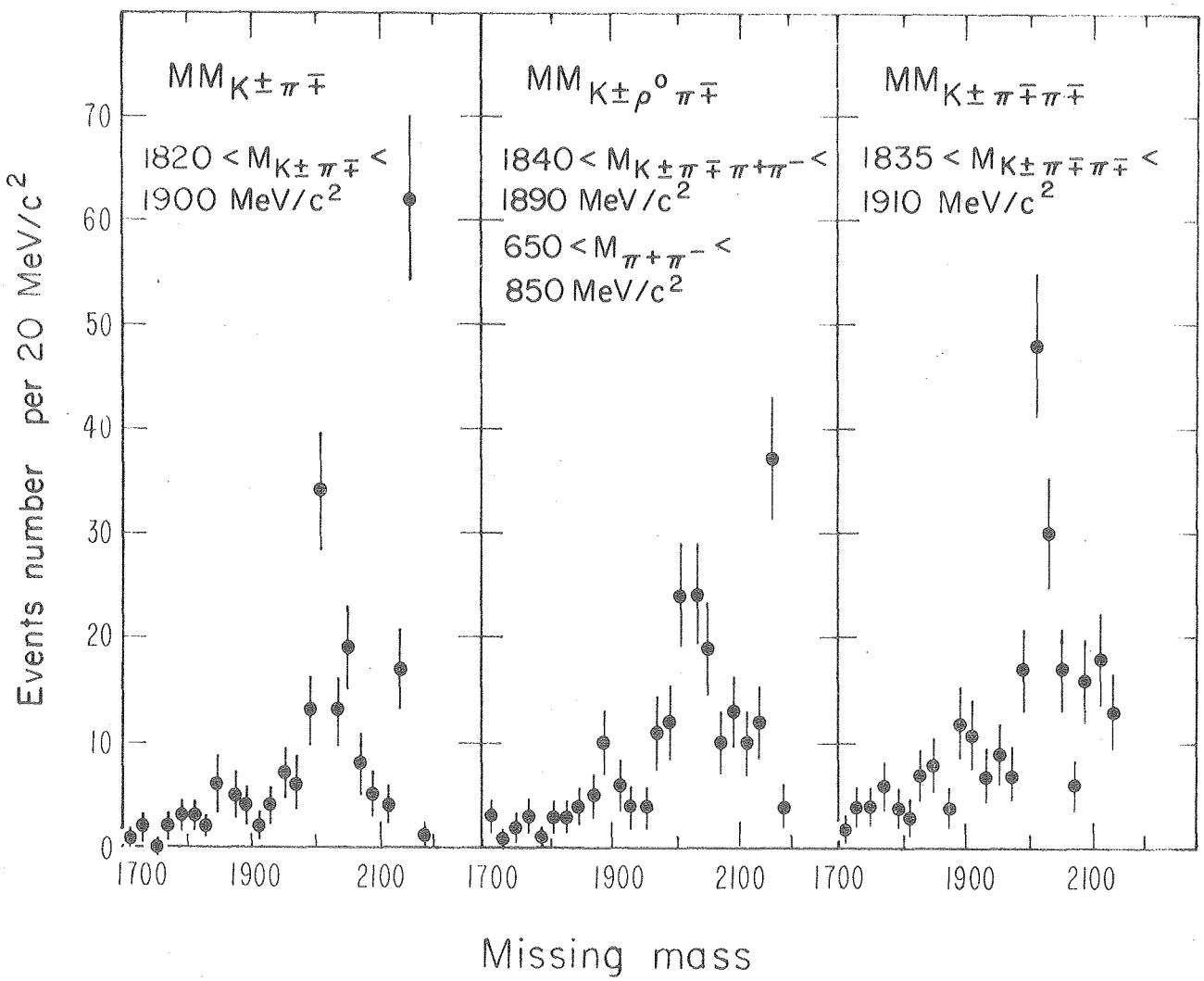

XBL 772-412

Fig. 8

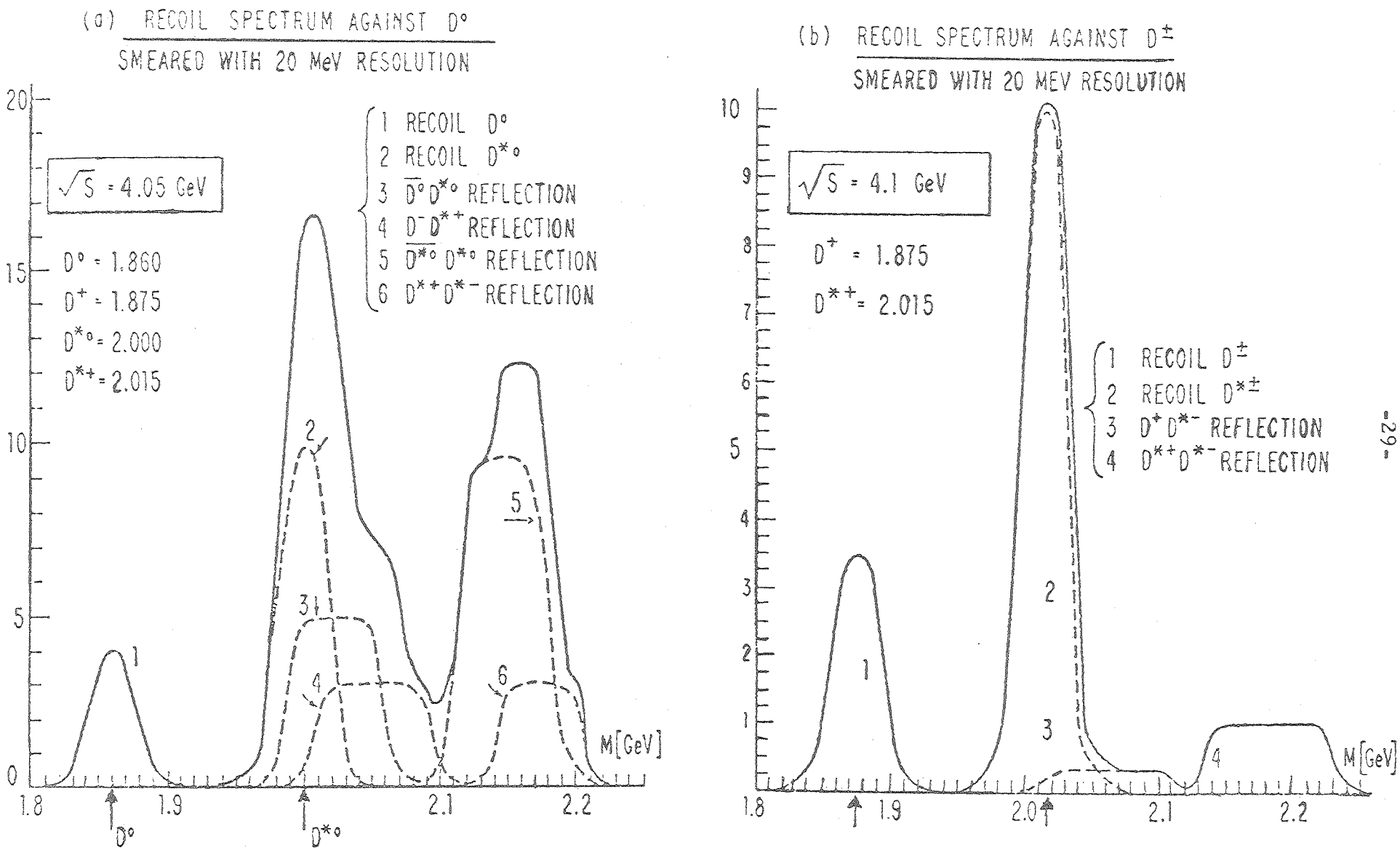

Fig. 9

XBL 773-8197

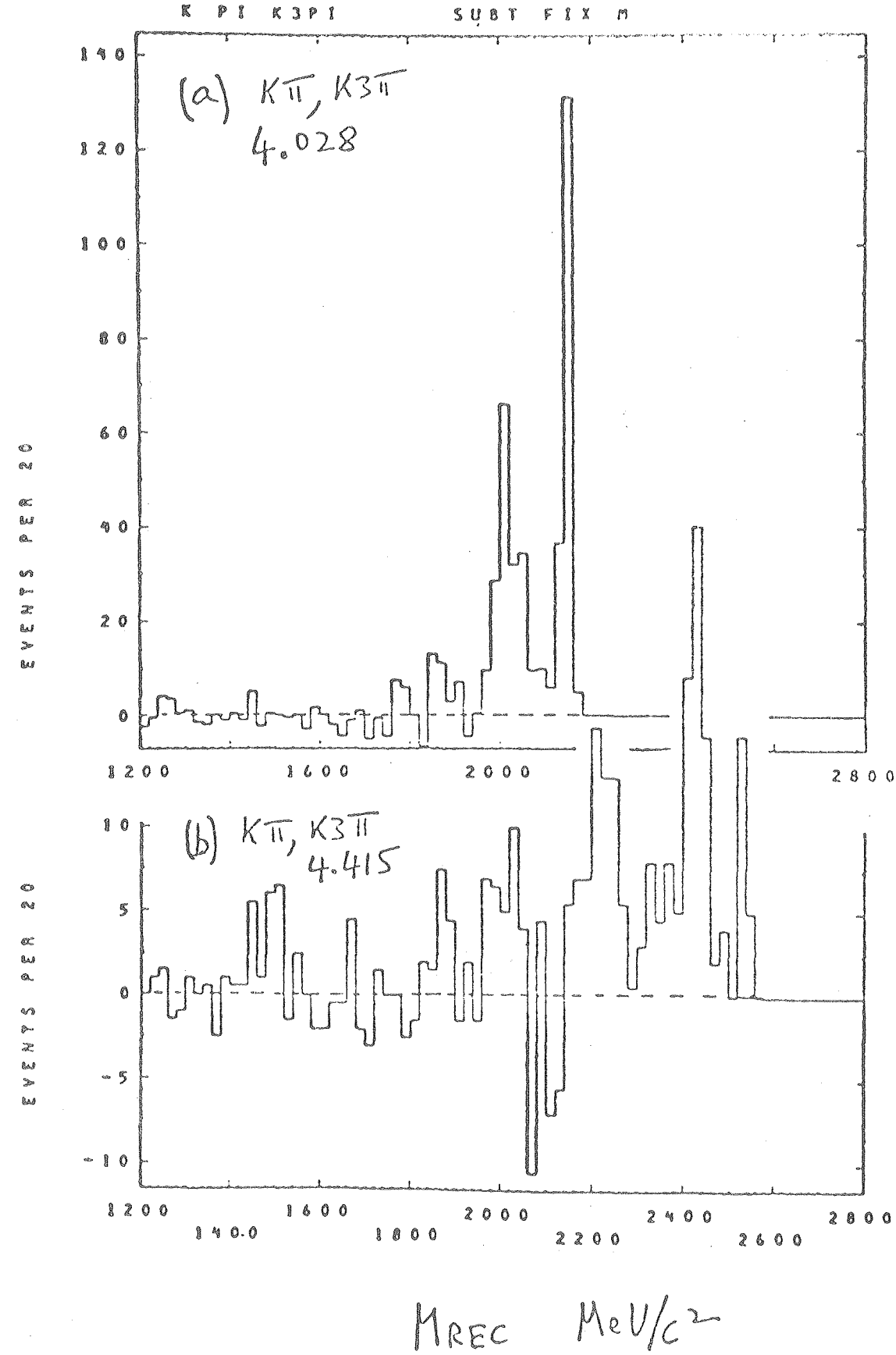

Fig. 10

XBL 773-8203

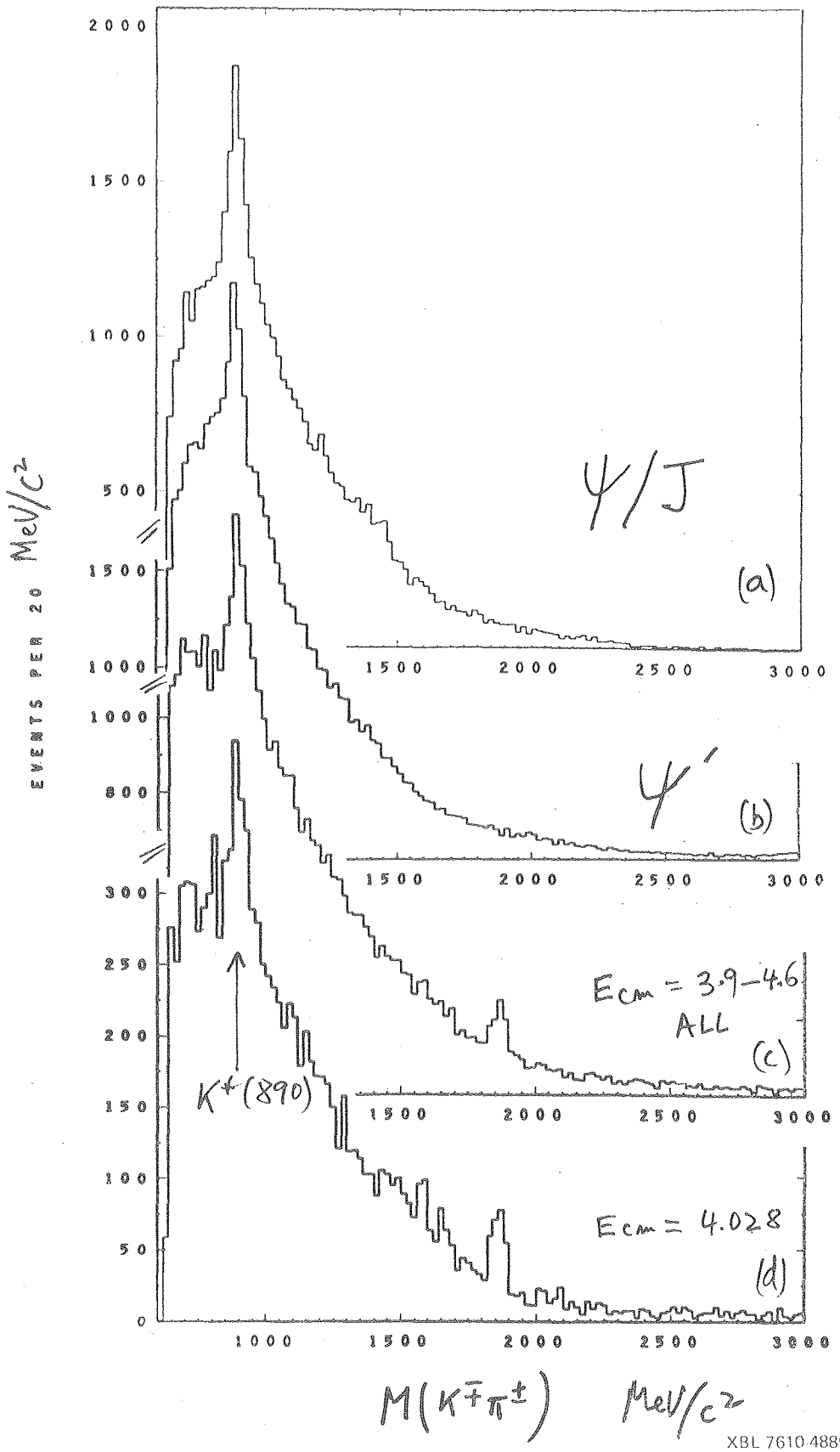

XBL 7610-4889

Fig. 11

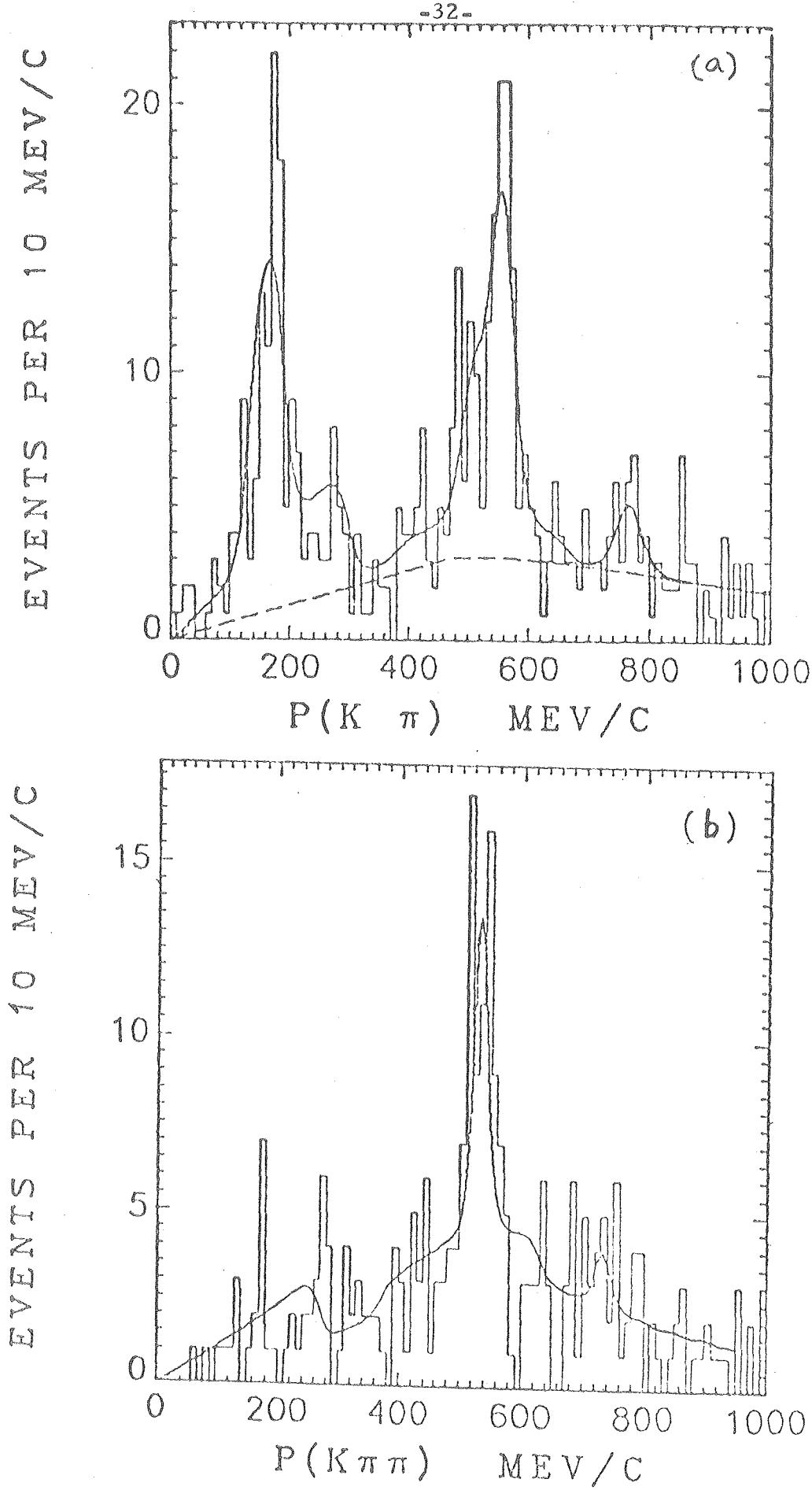

Fig. 12 XBL 773-8202

0 0 0 0 4 7 0 9 8 4 3

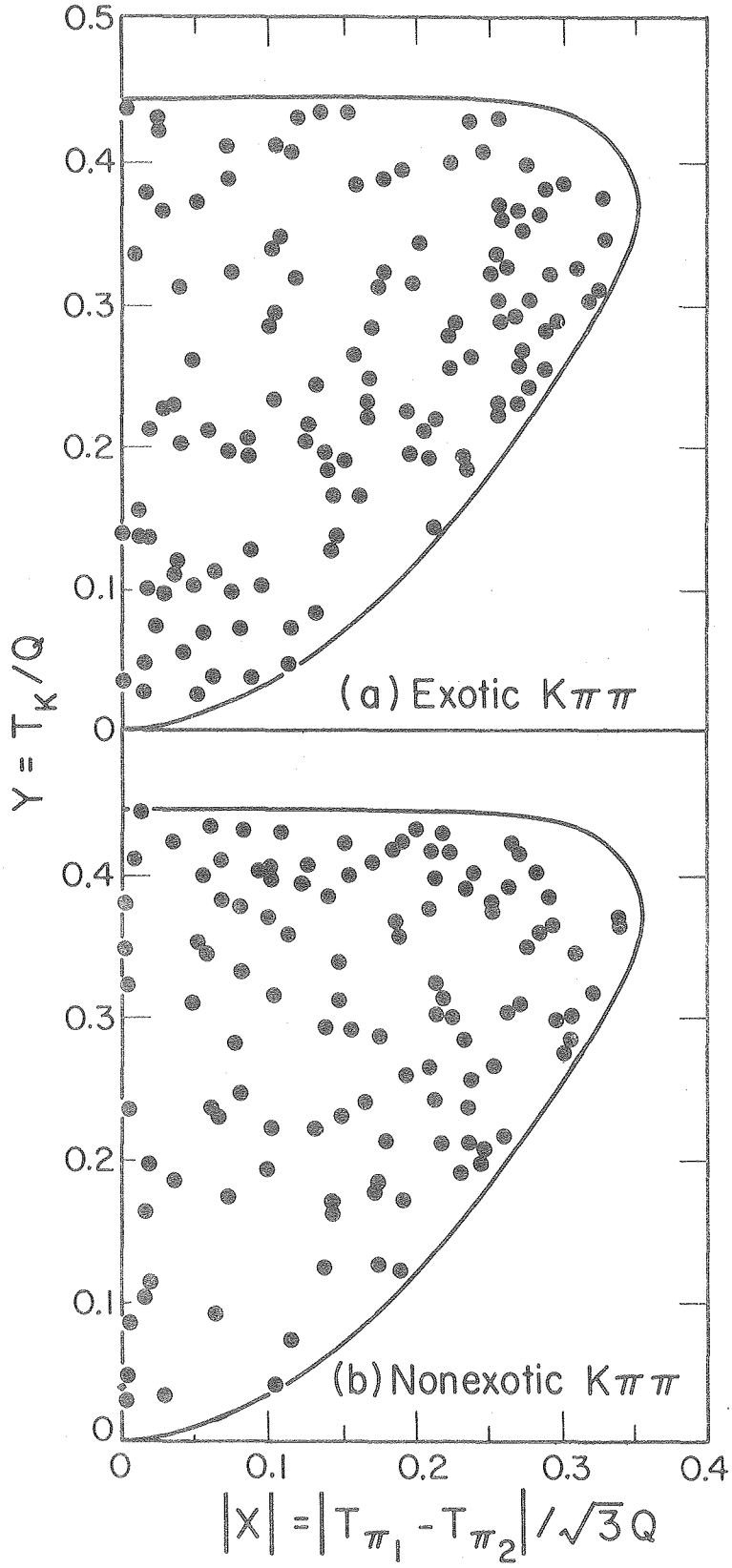

Fig. 13 XBL 7610-4116

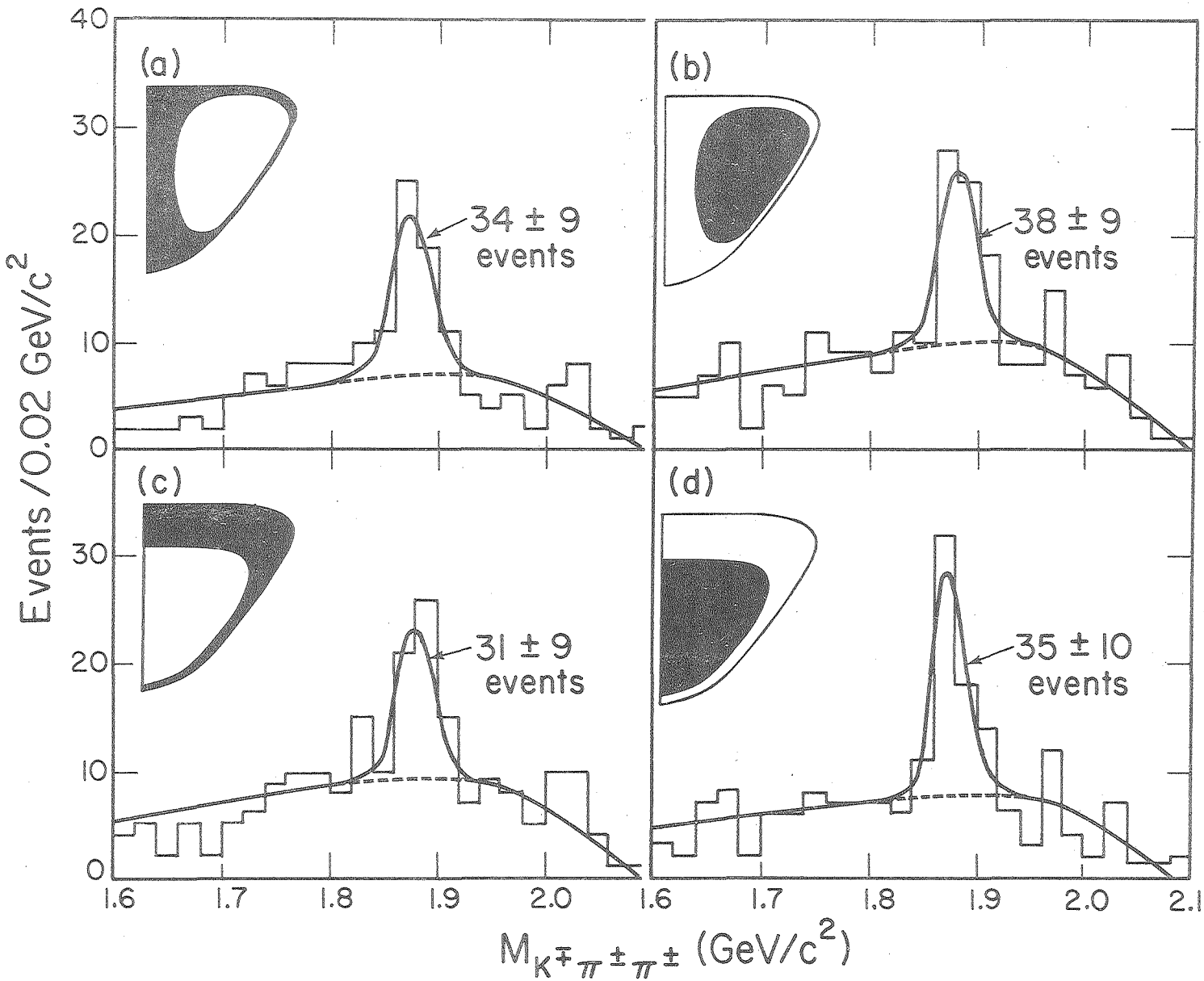

Fig. 14

XBL 7610 4114

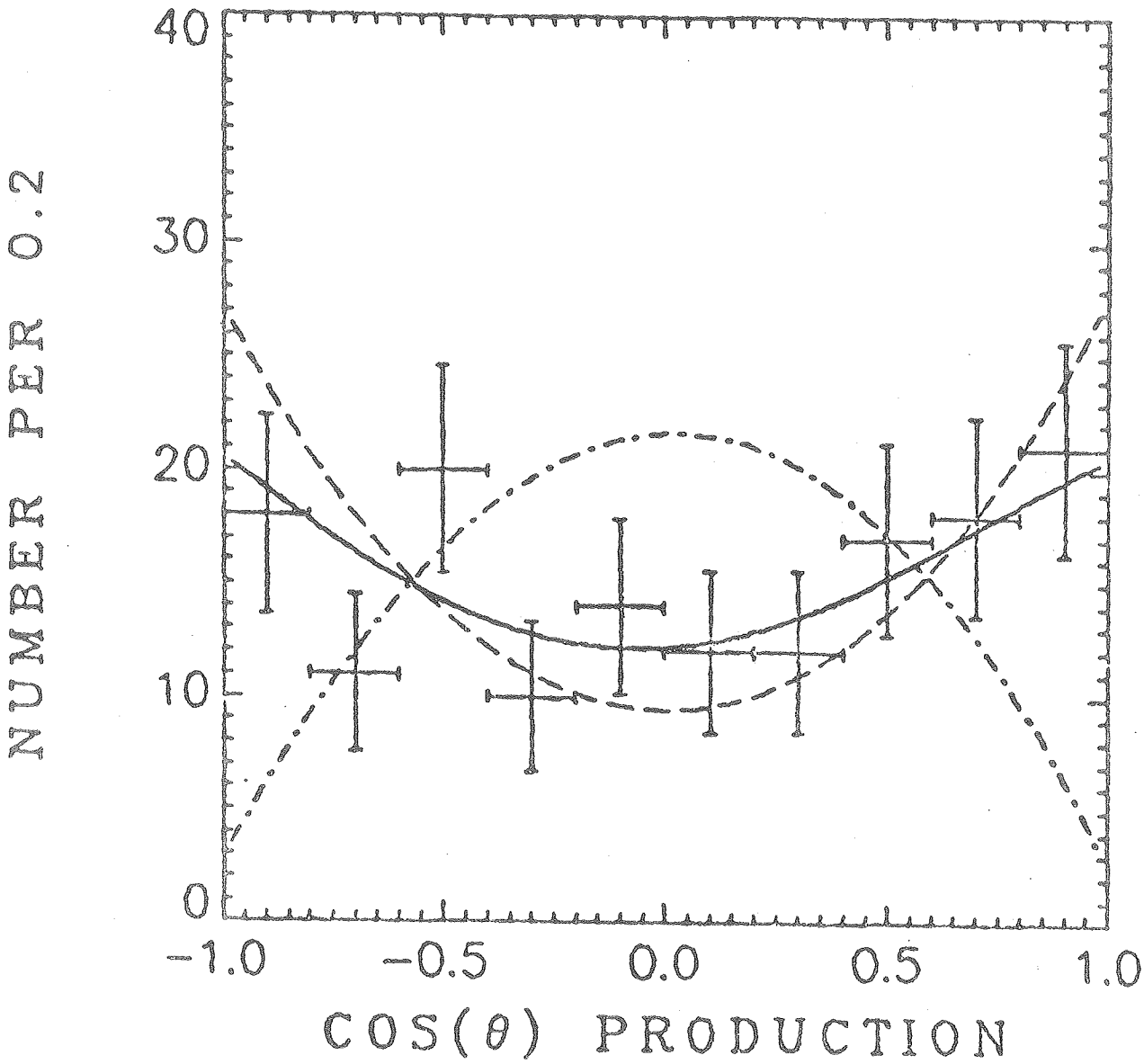

XBL 773-8204

Fig. 15

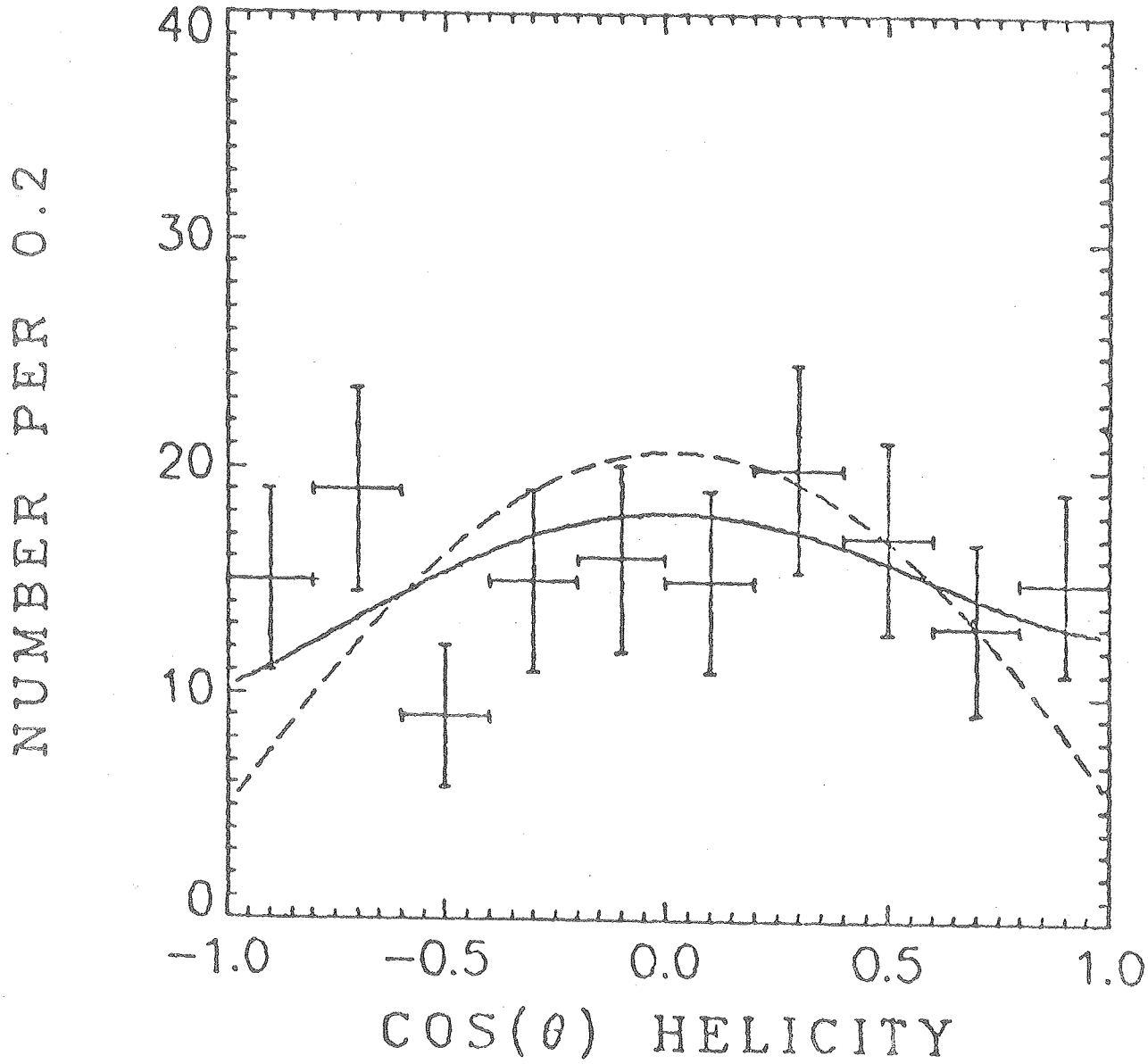

Fig. 16

XBL 773-8205

0 0 0 1 0 4 7 0 9 8 4 5

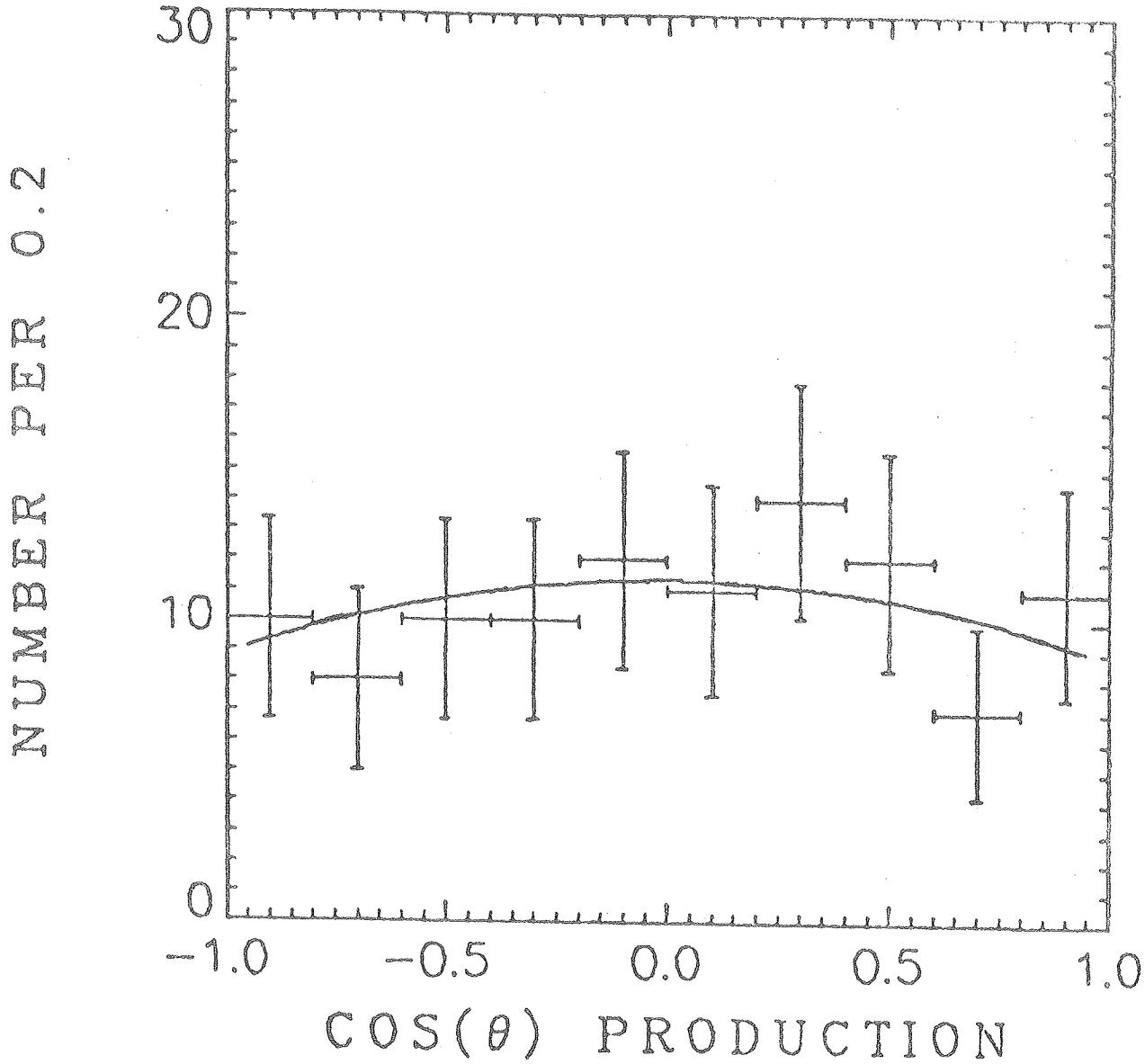

Fig. 17

XBL 773-8206

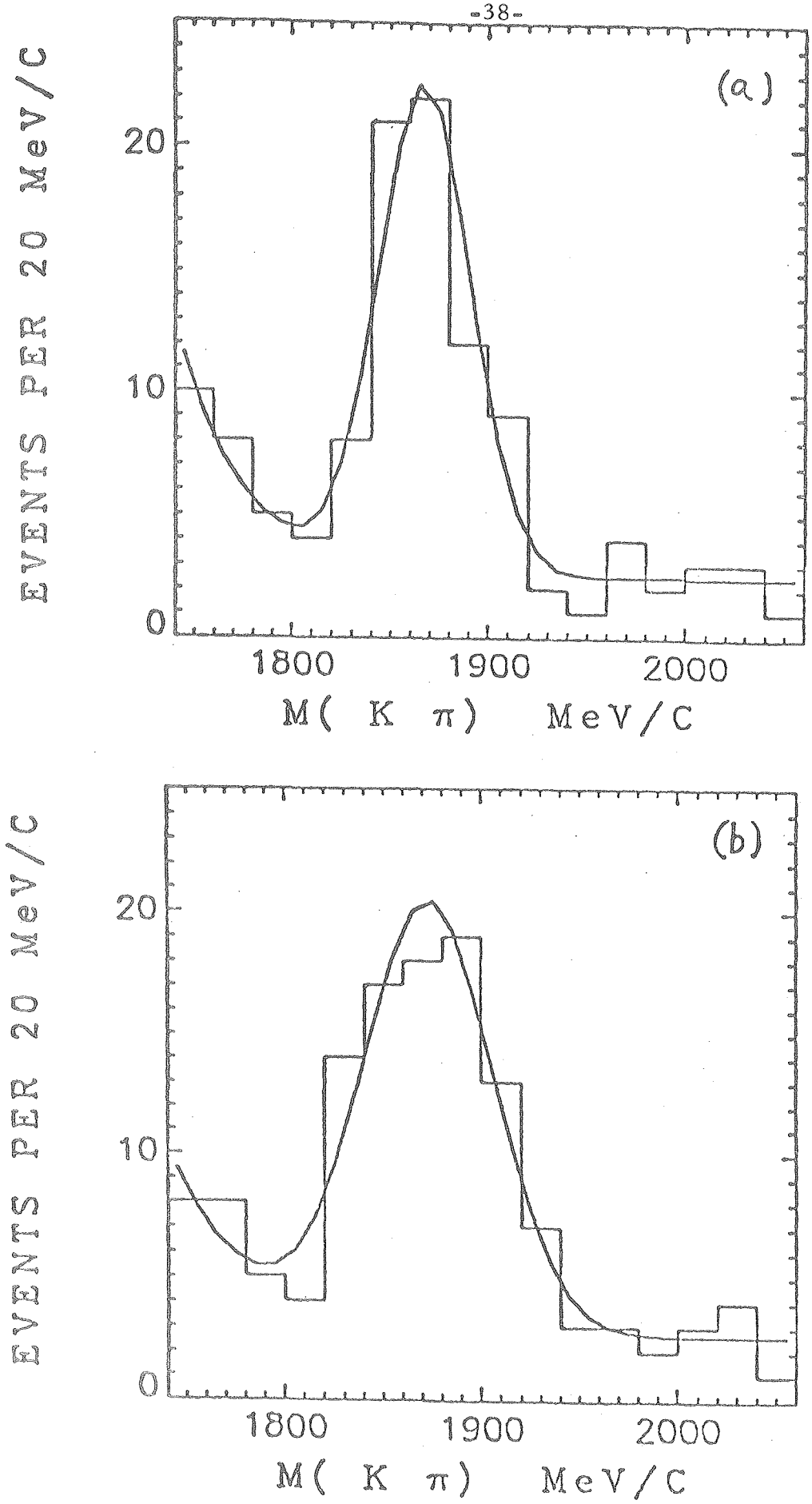

Fig. 18

XBL 773-8207

This report was done with support from the United States Energy Research and Development Administration. Any conclusions or opinions expressed in this report represent solely those of the author(s) and not necessarily those of The Regents of the University of California, the Lawrence Berkeley Laboratory or the United States Energy Research and Development Administration.

0 0 0 0 4 5 0 2 2 9 4